

Attention-aware Resource Allocation and QoE Analysis for Metaverse xURLLC Services

Hongyang Du, Jiazhen Liu, Dusit Niyato, *Fellow, IEEE*, Jiawen Kang, Zehui Xiong, Junshan Zhang, *Fellow, IEEE*, and Dong In Kim, *Fellow, IEEE*

Abstract—Metaverse encapsulates our expectations of the next-generation Internet, while bringing new key performance indicators (KPIs). Although conventional ultra-reliable and low-latency communications (URLLC) can satisfy objective KPIs, it is difficult to provide a personalized immersive experience that is a distinctive feature of the Metaverse. Since the quality of experience (QoE) can be regarded as a comprehensive KPI, the URLLC is evolved towards the next generation URLLC (xURLLC) with a personalized resource allocation scheme to achieve higher QoE. To deploy Metaverse xURLLC services, we study the interaction between the Metaverse service provider (MSP) and the network infrastructure provider (InP), and provide an optimal contract design framework. Specifically, the utility of the MSP, defined as a function of Metaverse users' QoE, is to be maximized, while ensuring the incentives of the InP. To model the QoE mathematically, we propose a novel metric named Meta-Immersion that incorporates both the objective KPIs and subjective feelings of Metaverse users. Furthermore, we develop an attention-aware rendering capacity allocation scheme to improve QoE in xURLLC. Using a user-object-attention level dataset, we validate that the xURLLC can achieve an average of 20.1% QoE improvement compared to the conventional URLLC with a uniform resource allocation scheme. The code for this paper is available at <https://github.com/HongyangDu/AttentionQoE>.

Index Terms—Attention-aware, Metaverse, resource allocation, contract theory, xURLLC

I. INTRODUCTION

A. Background

Initially, as a concept in fiction [1], Metaverse holds people's aspirations for the future world. The deployment of Metaverse services relies on the rapid advances of communication technologies. For example, Terahertz communications provide high data rate and low latency [2], advanced network techniques improve the security of Internet of Things (IoT) [3], [4], and multiple-input multiple-output (MIMO) technology further enhances the communication reliability. These promising techniques help to support key service areas in the

fifth-generation (5G) network architecture such as massive machine-type communications, enhanced mobile broadband, and ultra-reliable low-latency communications (URLLC) [5]–[7], thereby providing the technical basis for the implementation of Metaverse services. In particular, URLLC has great potential to support a series of significant Metaverse services based on graphical techniques such as virtual reality (VR) and augmented reality (AR), e.g., virtual traveling and meeting [8]. The reason is that these services require reliable transmission of user-object interactions and low latency delivery of virtual object data.

However, the emergence of Metaverse services and applications brings new key performance indicator (KPI) requirements that are different from those in the conventional URLLC services. Specifically, to provide users with an immersive experience in a deeply interactive environment of virtual and real worlds, graphical technology-enabled next-generation Internet services should have the ability to bring users personalized stimulation of various sense information. The “user-centric” requirement is difficult to be achieved solely by the conventional URLLC that focuses mainly on objective KPIs such as data rate and outage probability. This leads to the presentation of the next generation URLLC (xURLLC) [9] to fully consider the users' subjective feelings.

Therefore, novel yet sophisticated Metaverse xURLLC services need personalized service design, real-time interaction, and energy efficiency network availability, which places great demands on access technologies and novel user-centric resource allocation schemes [10]–[13]. For example, Metaverse xURLLC services, e.g., AR game, should ensure high quality in environment sensing, data transmission, and personalized graphic rendering to provide users an excellent feeling of immersion. To consider comprehensively the above multiple technical indicators and user feelings, we model the QoE to encompass significant KPIs in Metaverse xURLLC services, and take QoE as the service design goal.

To maximize QoE, we need to personalize the design of the resource allocation scheme according to the users' interest difference. This idea is also inspired by the recent successes in semantic communications [14]. By extracting and processing the semantic information from the data to be transmitted, several service KPIs can be greatly improved under the same resource constraints [15]. The reason is that more transmission resources can be allocated to the data related to the tasks. In Metaverse xURLLC services such as virtual traveling, meeting, and sports, the task of the Metaverse service provider (MSP) could be *providing users excellent Metaverse*

H. Du and D. Niyato are with the School of Computer Science and Engineering, Nanyang Technological University, Singapore (e-mail: hongyang001@e.ntu.edu.sg, dniyato@ntu.edu.sg). J. Liu is with the School of Information, Renmin University of China, China (e-mail: liujiazhen@ruc.edu.cn). J. Kang is with the School of Automation, Guangdong University of Technology, China. (e-mail: kavinkang@gdut.edu.cn). Z. Xiong is with the Pillar of Information Systems Technology and Design, Singapore University of Technology and Design, Singapore (e-mail: zehui_xiong@sutd.edu.sg). J. Zhang is with the Department of Electrical and Computer Engineering, University of California Davis, USA (e-mail: jzhang@ucdavis.edu). D. I. Kim is with the Department of Electrical and Computer Engineering, Sungkyunkwan University, South Korea (e-mail: dikim@skku.ac.kr).

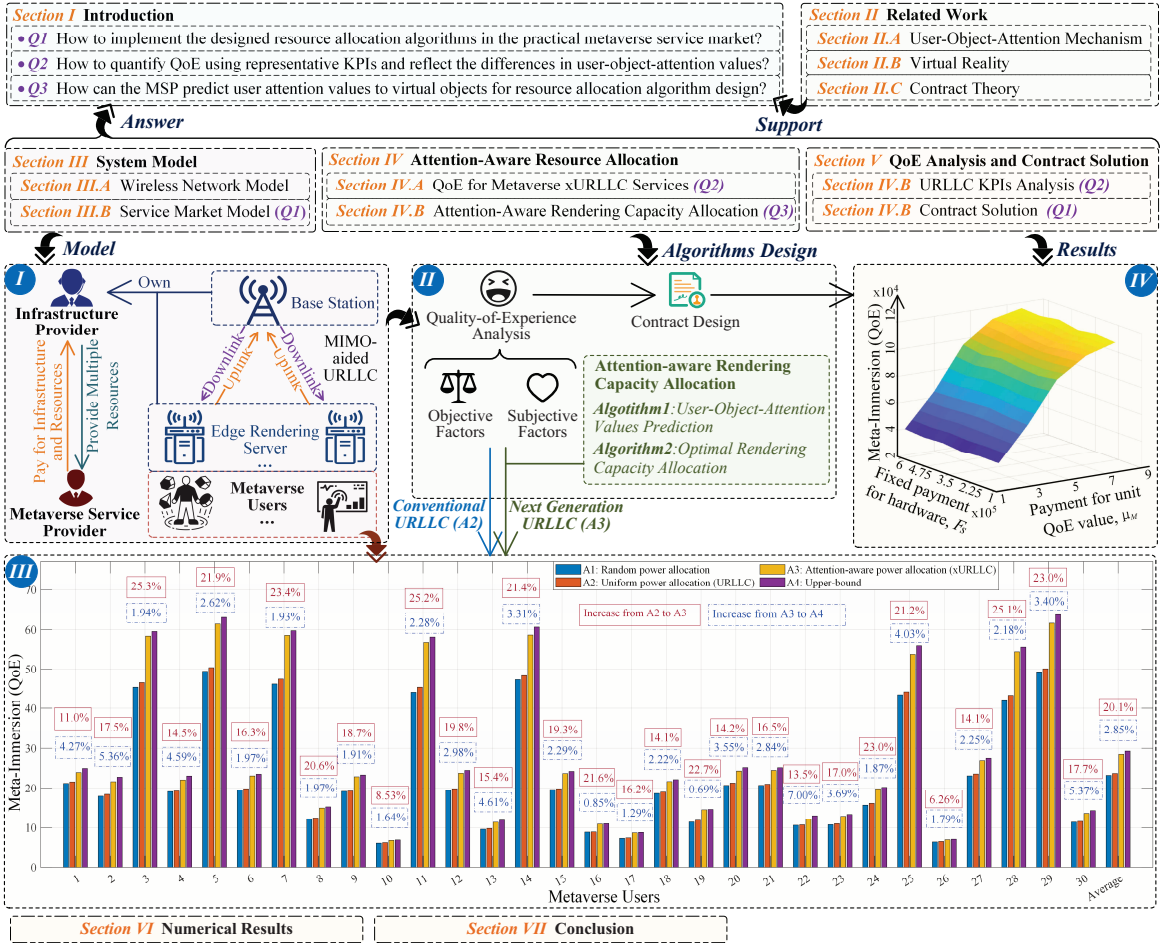


Fig. 1. Structure and main contributions of this paper. Part I shows the system model. Part II shows the ideas of QoE formulation and algorithms design. Part III shows that the Meta-Immersion of 30 users under three different resource allocation schemes, i.e., random, uniform (in conventional URLLC without considering the attention differences among users), attention-aware rendering capacity allocation (in xURLLC), and the upper-bound obtained from the ground truth. Part IV shows the Meta-Immersion versus the payment from the MSP to the network infrastructure provider (InP) for unit QoE value, u_M , and the fixed payment from the MSP for using the hardware infrastructures, F_s .

immersion experiences. Thus, by analyzing and predicting users' interests, we can allocate more network resources, e.g., rendering capacity, to virtual objects in which users will pay more attention, just as we allocate more transmission resources to the task-related data in semantic communications. Here we use the term "user-object-attention value" to express the user's interest in the virtual object. To implement the above Metaverse xURLLC service scheme, the following questions needs to be answered:

- Q1) How to implement the designed Metaverse xURLLC service scheme in the practical service market?
- Q2) How to quantify QoE using representative KPIs and reflect the differences in user-object-attention values?
- Q3) How can the MSP predict user attention values to virtual objects for resource allocation algorithm design?

To fill the aforementioned research gaps, we study the service market among the MSP, Metaverse users, and the InP, as shown in Fig. 1 (Part I). Because the Metaverse services are emerging businesses, the InP gains new opportunities to sell network resources to the MSP. From the MSP's perspective, it "employs" the InP to provide virtual services to users. There-

fore, a qualified mechanism should be designed to reward the InP comprehensively for driving the InP's incentives to take actions. Specifically, to maximize the utility of the MSP and ensure the InP agrees with the incentive scheme, we have to consider the incentive compatible (IC) constraint [16], which means that the InP provides the optimal amount of resources to maximize its own utility, and the individual rationality (IR) constraint [16], which means that the utility of the InP is larger than a threshold. To this end, contract theory can be a suitable solution for the incentive scheme design problem [17].

B. Contributions

We aim to design an MSP-InP contract¹ that weighs the InP's contributions by the QoE and maximizes the utility of the MSP. The main contributions of this paper are summarized as follows:

¹We focus on the contract design between one MSP and one InP [16], [17]. For the multiple InPs case, because the MSP can assign different services to different InPs, it is still an one-to-one contract design problem [17]. The case that multiple InPs compete one Metaverse service is left to future work.

- We introduce a new xURLCC service framework for Metaverse. By analyzing the physical edge network and the service market between the MSP and the InP, we propose a contract theory-based framework that takes both multidimensional network resources and the QoE into account. The utility of the MSP is maximized under the service market constraints while ensuring that the InP obtains a satisfactory incentive to participate in the contract (for **Q1**).
- For the proposed framework, we then design a novel metric named Meta-Immersion (MI) to model the QoE from the perspective of Metaverse users. By using the psychological Weber–Fechner Law, MI includes both objective service quality and subjective feelings of users. The MIMO technique is used to achieve URLLC. We then derive the closed-form expressions of downlink data rate and uplink bit error probability (BEP) to obtain MI expression in the xURLLC system (for **Q2**).
- With the MI metric, we further propose an attention-aware rendering capacity allocation algorithm to achieve xURLLC, which can predict users’ attention to all virtual objects through the historical sparse user-object-attention records and then allocate resources optimally (for **Q3**).
- To facilitate the quantification of QoE in a Metaverse context, we analyze the user-object-attention level (UOAL) dataset [18] that contains the attention values of 30 users to 96 objects. Using UOAL, we validate that the proposed xURLLC attention-aware allocation scheme can improve the QoE averagely by 20.1% compared to the conventional URLLC with the uniform resource allocation scheme. A higher percentage of QoE improvement, e.g., 40%, is achieved when the total resources for Metaverse xURLLC services are limited.

The structure of this paper is shown in Fig. 1. Section II reviews the related work in the literature. In Section III, we introduce the system model, which contains the wireless MIMO network and the service models. In Section IV, the QoE metric, i.e., MI, is formulated and the attention-aware resource allocation algorithms are proposed to achieve the xURLLC. In Section V, we derive the closed-form MI and obtain the contract solution. Section VI shows the effectiveness of our proposed schemes. Section VII concludes this paper.

II. RELATED WORK

This section provides a brief review of the related work on the user-object-attention mechanism, VR, and contract theory in the service market.

A. User-Object-Attention Mechanism

Eye-movements, the reliable mirror of attention allocation, are second nature of humans [19]. The authors in [20] find that, in the free-viewing of natural scenes, fixation duration is dependent mainly on attention ratings. Thanks to recent development in the field of head-mounted displays (HMDs) and computer graphics, pervasive eye trackers can be used easily to collect eye movement data [21]–[23]. A large amount of eye movement data is indeed useful for the personalized

service design [21]. In general, it has been shown that the eye movement data can be employed for the assessment of situational attention [21], detection of personality traits [22], and activity recognition even in challenging daily tasks [23]. Thus, the user-object-attention values can be obtained from eye movement records and help us make better use of rendering resources to achieve the xURLLC.

B. Virtual Reality

As one of the most significant enablers of 6G communications, VR demonstrates great potential as a key technology to access the virtual world, e.g., Metaverse [6]. With the rise of consumer-level VR devices, and especially HMDs with lower graphical compute capabilities, one obstacle, which is hard to be solved in conventional URLLC, is to achieve high virtual object quality at a low cost. To solve this problem, the authors in [24] optimize video streaming with the help of eye-tracking. A hidden Markov model is used to predict the user’s gaze region that is then encoded in higher quality than the rest. It is shown that 29% bitrate savings can be achieved without the users reporting quality degradation. Similarly, the authors in [25] adopt the virtual content in real-time according to the user’s gaze. However, allocating resources based on user gaze behavior requires real-time computing and ignores the interest of users, i.e., attention to virtual objects. Thus, a better option is to allocate rendering capacity, e.g., in the form of resolution, based on the user’s attention to different virtual objects. In fact, some literature discusses the adaptive resolution method in VR. A mechanism that can adjust the VR resolution according to task complexity is proposed in [26]. Moreover, the authors in [27] discuss the adaptive resolution-based trade-offs for energy-efficient visual computing systems.

C. Contract Theory

Contract theory has been widely used in wireless networks [28]. To the best of our knowledge, the authors in [29] first apply contract theory to the spectrum sharing problem. Since then, the contract theory is used in a growing number of problems, e.g., D2D communications [30], data transactions [30], and energy management [31]. The book [16] studies and summarizes the use of contract theory in wireless networks, and discusses the multi-contract design and the one-to-one contract optimization between two entities. The latter is used as the incentive mechanism in crowd-sourcing to maximize the utility of the principal while providing the users continuous incentives [17]. However, the cooperation patterns are impacted by the recent development of wireless networks, in which multiple resources can be used [32]. Furthermore, the optimal contract design is decided by the QoE. The contract design between the MSP and the InP of the wireless network has not been fully investigated.

Inspired by these existing works, we apply contract theory to study the cooperation between the MSP and the InP in the Metaverse service market, and design an attention-aware resource allocation scheme to maximize the QoE.

III. SYSTEM MODEL

With the help of wireless network infrastructures owned by the InP, the MSP can rapidly deploy Metaverse applications and services to improve the QoE of users. We consider one of the basic Metaverse xURLLC services: *Providing users with virtual immersion experiences*, such as virtual traveling and meeting [33]. In this kind of services, there are several options for users, e.g., different virtual traveling scenarios. In this section, we first present the wireless network for Metaverse xURLLC services, and then discuss the service market model between the MSP and the InP.

A. Wireless Network Model

In wireless MIMO networks, multiple antennas are adopted at both the transmitter and receivers to obtain considerable array gains and improve the channel quality. As shown in Fig. 1 (Part I), we consider that a multi-antenna cloudlet-enabled base station (CBSs) can use the wireless communication resources, i.e., transmit power and bandwidth, to interact with the edge devices. Multi-antenna edge devices, such as rendering servers (RSs), receive the downlink virtual object data and render objects for users.

Wireless environments have a significant impact on Metaverse xURLLC service quality. Strong small-scale fading and severe interference from other co-channel users result in the InP using more resources to maintain the same QoE as when the wireless environment is favorable. Here we study the wireless connections between CBSs and RSs, considering the effects of number of antennas, small-scale and large-scale fading, transmit power, number of co-channel interference paths, and interference power. Because the RS can be placed in the user's home or integrated into the HMD, we consider one RS serves one user [34]. With the network parameters shown in Table I, we express the probability density function (PDF) of the signal-to-interference ratio (SIR) under the interference-limited scenario for the k_{th} ($k = 1, \dots, M_U$) user as [35]

$$f_{\gamma_k}(\gamma) = \frac{\Lambda_k(\gamma\Lambda_k)^{M_C M_U - 1}}{B(M_C M_U, M_C N_Q)(1 + \gamma\Lambda_k)^{M_C M_U + M_C N_Q}}, \quad (1)$$

where

$$\Lambda_k \triangleq \frac{P_{k,q}\mu_{k,q}}{M_C \zeta_k D_k^{-\alpha_k} P_k^{(D)} \mu_k}, \quad (2)$$

$$\zeta_k = \mathbb{E}[\lambda_{\max}] / \mathbb{E}\left[\sum_{i=1}^{\min\{M_C, M_U\}} \lambda_i\right], \quad (3)$$

λ_i ($i = 1, \dots, \min\{M_C, M_U\}$) are the non-zero eigenvalues of the matrix $\mathbf{H}_k^H \mathbf{H}_k$, λ_{\max} is the largest eigenvalue, $\mathbb{E}[\cdot]$ represents statistical expectation, and $B(\cdot, \cdot)$ is the Beta function [36, eq. (8.384.1)]. With the help of (1), we mathematically analyze the objective service KPIs in Section IV-A which impact the QoE of Metaverse users and the utilities of the InP and the MSP.

The wireless network architecture leads to a new market value chain comprising the InP, the MSP, and users. The InP's input of physical infrastructures, computing, and communi-

TABLE I
WIRELESS COMMUNICATIONS NETWORK PARAMETERS.

Notation	Network Parameter
M_C	Number of antennas in CBS
M_U	Number of antennas in RS
N_U	Number of Metaverse users
N_Q	Number of co-channel interference paths
D_k	Transmission distance between the j_{th} CBS and k_{th} user
α_k	Path loss exponent between the j_{th} CBS and k_{th} user
$P_k^{(D)}$	Downlink transmit power
$P_{k,q}$	Interference power
$\mathbf{H}_k \in \mathbb{C}^{M_U \times M_C}$	Channel between the k_{th} user and the j_{th} CBS
μ_k	Rayleigh channel coefficient of data links
$\mu_{k,q}$	Rayleigh channel coefficient of interference links

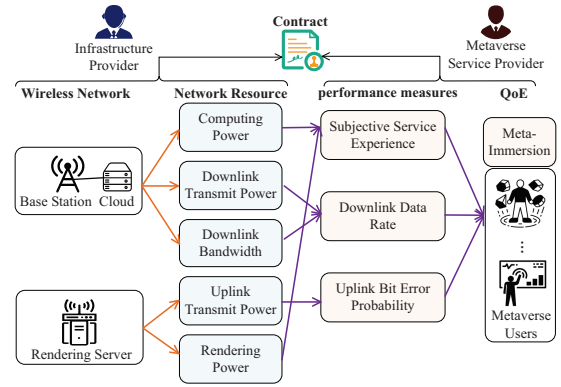


Fig. 2. A contract theory-based Metaverse xURLLC service market with multi-dimension resources and the QoE-based payment.

cation resources helps the MSP deploy Metaverse xURLLC services to users, and the MSP needs to pay the InP.

B. Service Market Model

We study the contract theory-based payment plan in this section. The utilities of the InP and the MSP are formulated respectively, by considering the QoE of Metaverse users.

1) *Payment Plan*: To realize the full potential of the wireless network, an appropriate payment plan is required, which allows all stakeholders and Metaverse xURLLC service users to benefit from the cooperation. We propose a contract theory-based payment plan, in which the InP receives the fee from the MSP according to the computing and communication resources that the InP provides and the QoE of MSP's users. Thus, the revenue function of the InP can be expressed as

$$I_{\text{InP}} = F_s + u_M \sum_{i=1}^{N_U} \mathcal{M}_i, \quad (4)$$

where F_s is the fixed payment from the MSP for using the hardware infrastructures, u_M is the fee for unit QoE value, and \mathcal{M}_i is the value of the quantified QoE of i_{th} Metaverse

user. Note that \mathcal{M}_i is determined by various resources of the InP as well as by the user's personalized subjective parameters, which is discussed in detail in Section IV-A.

2) *Utility of the InP*: As shown in Fig. 2, the InP invests multidimensional network resources, i.e., downlink transmit power $P_k^{(D)}$, downlink bandwidth B_k , uplink transmit power $P_k^{(U)}$, and rendering capacity $P_k^{(R)}$, which are denoted by

$$\Theta = \left(P_k^{(D)}, B_k, P_k^{(U)}, P_k^{(R)} \right). \quad (5)$$

Then, the InP's cost is defined in a quadratic form as $\|\mathbf{u}_\Theta \odot \Theta\|^2$, where \odot means the Hadamard product [37], $\mathbf{u}_\Theta = (\sqrt{u_{1\theta}}, \dots, \sqrt{u_{N\theta}})$, and $u_{i\theta}$ is the cost for the i_{th} unit resource [16]. These resources impact the KPIs of the Metaverse xURLLC services. Here we study three types of KPIs, i.e., downlink data rate $R_k^{(D)}$, uplink BEP $E_k^{(U)}$, and subjective service experience X_k , which are denoted by

$$\Psi = \left(R_k^{(D)}, E_k^{(U)}, X_k \right). \quad (6)$$

Note that X_k indicates the subjective feeling of users towards xURLLC service that is discussed in Section IV-A. $R_k^{(D)}$ and $E_k^{(U)}$ are objective conventional URLLC KPIs that are considered due to the following two facts:

- The VR data delivery requires high downlink data rate to ensure low transmission latency.
- For the data uplink, the data amount is not large, but small bit error probability should be ensured to achieve accurate user-object interactions [38].

Our analysis framework can be extended easily when other types of KPIs are considered.

The Metaverse xURLLC service is an emerging business with uncertainty, which may lead to the situation that the InP is not certain to be profitable from cooperation with the MSP. Specifically, the demands of users depend highly on socio-economic factors such as the popularity of the MSP among their friends [39]. This motivates us to consider the user risk preference [40] in the InP utility. A measure of risk aversion that is commonly used in financial economics is the Arrow-Pratt measure of relative risk aversion (RRA) [40], as

$$\text{RRA} = -\frac{U''_{\text{InP}}(W_{\text{InP}})}{U'_{\text{InP}}(W_{\text{InP}})} W_{\text{InP}}, \quad (7)$$

where

$$W_{\text{InP}} \triangleq I_{\text{InP}} - \|\mathbf{u}_\Theta \odot \Theta\|^2, \quad (8)$$

is the difference between the revenue and cost, and $U_{\text{InP}}(W_{\text{InP}})$ is the utility of the InP. The RRA measures the degree of risk aversion of the InP under consideration, where a larger RRA means more risk aversion. Here we consider that the InP has constant relative risk aversion (CRRA) preferences for the Metaverse services. Then, a common utility function in economics with CRRA is the power utility as [40]

$$U_{\text{InP}}(W_{\text{InP}}) = \frac{W_{\text{InP}}^{1-\tau}}{1-\tau}, \quad (9)$$

where τ is the value of RRA when substituting (9) into (7). Typically, the contract between the MSP and the InP is designed to ensure that the utility of the InP is larger than a

certain threshold. Thus, we consider $0 \leq \tau < 1$. Note that, for $\tau = 0$, we can rewrite (9) as $U_{\text{InP}}(W_{\text{InP}}) = W_{\text{InP}}$, which means that the preference of the InP shows risk neutrality.

3) *Utility of MSP*: Since the MSP is typically a well-established business, e.g., Facebook, and is more tolerant to the uncertainties, we consider that the MSP is risk neutral, and express the utility of the MSP as

$$U_{\text{MSP}} = \sum_{i=1}^{N_U} (\omega_{U_i} + \mu_{U_i} \mathcal{M}_i) - I_{\text{InP}}, \quad (10)$$

where ω_{U_i} represents the basic fee paid by the i_{th} user for access to Metaverse, and μ_{U_i} denotes the additional fee of virtual services, e.g., the user pays for the high-quality access service to obtain higher QoE [41].

Remark 1. We observe that the utilities of both InP and MSP increase if the QoE of Metaverse users can be increased under the same resource investment. The reason is that the InP can gain more payments at the same amount of resources cost, and the MSP can attract more users by providing higher QoE.

As such, we now analyze the QoE from the rendering quality perspective, i.e., X_k in (6) denotes the rendering quality that users perceive. In Metaverse, through VR access, a user will perceive and put attention to different displayed objects differently. For example, the user may have more attention to persons' avatars rather than a table in a virtual meeting. Thus, it is more efficient to use higher rendering capacity on objects of greater interest to the user. To facilitate such resource allocation, we predict the user's attention to objects to be displayed in Section IV, using the sparse historical records of objects seen by the user before.

4) *Optimal Contract Design*: Combing (9), (10), (4), and (8), we can express the utility functions of the MSP and the InP as

$$U_{\text{MSP}}(\Theta, F_s, u_M) = \sum_{i=1}^{N_U} (\omega_{U_i} + (\mu_{U_i} - u_M) \mathcal{M}_i) - F_s, \quad (11)$$

and

$$U_{\text{InP}}(\Theta, F_s, u_M) = \frac{1}{1-\tau} \left(F_s + u_M \sum_{i=1}^{N_U} \mathcal{M}_i - \|\mathbf{u}_\Theta \odot \Theta\|^2 \right)^{1-\tau}, \quad (12)$$

respectively. The contract provided by the MSP includes two items, i.e., $\{F_s, u_M\}$. To design the optimal contract, we formulate the MSP's utility maximization problem while providing the InP with the necessary incentives to agree on the contract. The optimization problem can be expressed as [17]

$$\begin{aligned} & \max_{\Theta, F_s, u_M} U_{\text{MSP}}(\Theta, F_s, u_M) \\ & \text{s.t.} \quad \begin{cases} \Theta^* \in \arg \max_{\Theta} U_{\text{InP}}(\Theta, F_s, u_M), \\ U_{\text{InP}}(\Theta^*, F_s, u_M) \geq U_{\text{th}}^{\text{InP}}, \end{cases} \end{aligned} \quad (13)$$

where the first constraint is the IC constraint [16], i.e., $P_k^{(D)*}$, B_k^* , $P_k^{(U)*}$, and $P_k^{(R)*}$ is set to maximize its own utility. The second is the IR constraint [16] with a utility threshold $U_{\text{th}}^{\text{InP}}$.

This contract design problem can be viewed as a leader-follower game model, which can be easily solved if we know

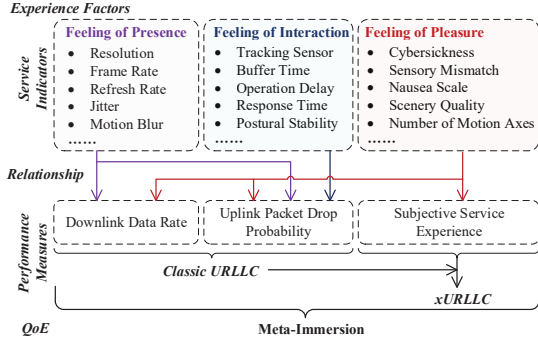


Fig. 3. A novel performance metric in Metaverse: Meta-Immersion, and corresponding experience factors, service indicators, and KPIs, a.k.a., performance measures.

the value of Θ under each $\{F_s, u_M\}$ [42]. Here, Θ is designed to maximize the utility of the InP, which is equivalent to maximizing \mathcal{M}_i . Thus, we need to obtain the closed-form expression for the QoE of the i_{th} user (**Q2** in Section I), i.e., \mathcal{M}_i , and an optimal resource allocation scheme that maximizes \mathcal{M}_i to provide high-quality Metaverse xURLLC services (**Q3** in Section I).

IV. ATTENTION-AWARE RESOURCE ALLOCATION

In this section, we propose a novel metric termed MI using the Weber-Fechner Law [43], to model the user's QoE in Metaverse xURLLC service. To help the InP make effective use of resources, we propose a two-step attention-aware rendering capacity allocation algorithm.

A. QoE Analysis for Metaverse xURLLC Services

In the Metaverse service, three feelings, i.e., the feeling of presence, feeling of interaction, and feeling of pleasure, are important to the users' engagement [44]. As shown in Fig. 3, to quantify these feelings and corresponding service indicators, we consider three KPIs, i.e., downlink data rate $R_k^{(D)}$, uplink BEP $E_k^{(U)}$, and subjective service experience, to present the formulation of the QoE.

Note that downlink data rate and uplink BEP are objective KPIs in conventional URLLC that impact the interaction between the physical and virtual worlds, and the subjective service experience indicates the perceived quality of Metaverse service. For Metaverse xURLLC service studied in this paper, e.g., virtual traveling, we consider that the subjective service experience is decided by the rendering quality. Thus, let $P_{n,k}^{(R)}$ denote the rendering capacity and N_{O_k} denote the number of virtual objects that the k_{th} user sees in one service. The subjective service experience is a function of $P_{n,k}^{(R)}$ and N_{O_k} .

To establish the relationship between the network performance and the subjective experience, we use the Weber-Fechner Law to derive the QoE, i.e., MI, as the *connection coefficient* multiplied by the *logarithm of stimulus intensity* [45]–[47]. In Metaverse virtual services, the stimulus intensity can be expressed in terms of the rendering capacity. The *connection coefficient* is decided by the URLLC KPIs.

Then, the differential of the MI of the k_{th} user can be expressed as

$$d\mathcal{M}_k = C_k \sum_{n=1}^{N_{O_k}} K_{n,k} \frac{dP_{n,k}^{(R)}}{P_{n,k}^{(R)}}, \quad (14)$$

where $K_{n,k}$ is the user-object-attention value that is a constant determined by users' physiological mechanism and subjective attention, C_k is the *connection coefficient*. As we discussed in Section III-B2, we consider the downlink data rate and the uplink BEP as the conventional URLLC KPIs. Thus, C_k can be expressed as

$$C_k = \mathcal{T}(R_k^{(D)}) \mathcal{T}(1 - E_k^{(U)}). \quad (15)$$

The function $\mathcal{T}(\cdot)$ is used to eliminate the effect of the magnitudes [48], which is defined as

$$\mathcal{T}(t) = \frac{t - t_{\min}}{t_{\max} - t_{\min}}, \quad (16)$$

where t_{\min} is the minimal threshold, t_{\max} is the maximal value that InP can provide. From (14), we can observe that, unlike traditional psychological models, the stimulus perceived by the user is from Metaverse, and the transformation from the stimulus to the user's subjective feelings is influenced by the interaction between the virtual and the real worlds.

By solving (14), we obtain the MI for the k_{th} user as

$$\mathcal{M}_k = \mathcal{T}(R_k^{(D)}) \mathcal{T}(1 - E_k^{(U)}) \sum_{n=1}^{N_{O_k}} K_{n,k} \ln \left(\frac{P_{n,k}^{(R)}}{P_{\text{th}}^{(R)}} \right), \quad (17)$$

where $P_{\text{th}}^{(R)}$ is the minimal rendering capacity threshold, e.g., the resolution that is set for the object with the lowest attention.

Remark 2. Different Metaverse URLLC services have different focus on KPIs. For example, in instant virtual meeting services, latency could be a significant performance metric. Fortunately, our proposed QoE metrics can be adapted to different service design requirements by adjusting for the connection coefficient, i.e., C_k . For example, when latency, i.e., L_k , is considered in the QoE modelling, we can multiply $\mathcal{T}(L_{\max} - L_k)$ in C_k , where L_{\max} is the maximum delay that Metaverse service can tolerate.

Remark 3. In conventional URLLC, the goal of network service design is to achieve optimal objective performance metrics, such as higher downlink data rate and lower BEP. Although $\mathcal{T}(R_k^{(D)}) \mathcal{T}(1 - E_k^{(U)})$ in (17) can approach 1, the rendering capacity is typically allocated uniformly without utilizing the user's attention mechanism in Metaverse services, which limits the further improvement of QoE. Thus, in xURLLC, unlike the uniform allocation scheme in URLLC, we design the personalized attention-aware rendering capacity allocation scheme as follows.

B. Attention-Aware Rendering Capacity Allocation

There are two steps in the optimal rendering capacity allocation scheme. We first predict the user-object-attention values, i.e., $K_{n,k}$. Next, we design the optimal rendering

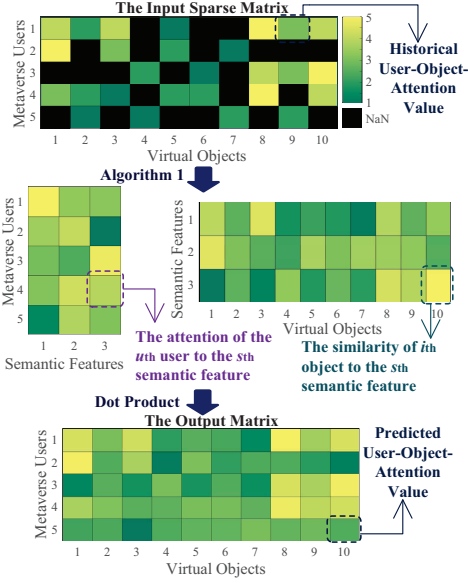


Fig. 4. The working principle of attention-aware user-object-attention values prediction.

capacity allocation scheme to maximize the MI given with predicted $K_{n,k}$. In the following, we design algorithms for the two steps, respectively.

1) *User-Object-Attention Values Prediction*: Because Metaverse users have different attention to different virtual objects, and labels of objects are available to the MSP, we consider the virtual objects as *observed features* of users. The user’s historical attention records to *observed features* are sparse [49], because the user has unseen objects. Clearly, we can cluster a group of objects with semantic relevance into a “topic”. The “topics” can be regarded as *semantic features*. For example, in the UOAL dataset, we have 96 virtual objects such as “mirror”, “ball”, “box”, and “poster”, the *semantic features* could be “toys”, “tools”, etc. Although we cannot divide objects into independent “topics”, it is reasonable to obtain a matrix that shows the similarities of each object to all semantic features. For example, “mirror” and “box” have high similarity to “tools” and low similarity to “toys”, “ball” is the reverse, and the similarities of “poster” to both “tools” and “toys” are low, but might be relatively higher to “toys”. Note that we do not need to consider the real meaning of *semantic features*, we only need to input the number of *semantic features*. As shown in Fig. 4, if we can estimate accurately the attention of users to *semantic features*, we can obtain the complete user-object-attention matrix by dot production [49].

Based on the above discussion and motivated by the matrix factorization method [49], we map Metaverse users and virtual objects into a joint semantic space that has S features. Then, the user-object-attention values can be modeled as inner products in the semantic space. Specifically, let N_U and N_O denote the number of users and objects in a user-object-attention matrix $\mathbf{A} \in \mathbb{R}^{N_U \times N_O}$, respectively. The semantic factor matrix for users and objects then can be expressed as $\mathbf{M} \in \mathbb{R}^{N_U \times S}$ and $\mathbf{N} \in \mathbb{R}^{N_O \times S}$, respectively. The set of objects that have historical attention records with the u_{th} user is denoted by

\mathcal{A}_u . Similarly, for the i_{th} object, the set of Metaverse users that have attention records is denoted by \mathcal{A}_i . The semantic feature vectors for the u_{th} user and the i_{th} virtual object are denoted by $\mathbf{m}_u \in \mathbb{R}^{S \times 1}$ and $\mathbf{n}_i \in \mathbb{R}^{S \times 1}$, respectively. Thus, the element a_{ui} in \mathbf{A} can be estimated as [49]

$$\hat{a}_{ui} = \mathbf{m}_u^T \mathbf{n}_i. \quad (18)$$

A weighted regression function-based method was proposed in [50] to learn the unknown model parameters. Similarly, we can obtain the predicted element \hat{a}_{ui} by minimizing the following function:

$$J = \sum_{u=1}^{N_U} \sum_{i=1}^{N_O} w_{ui} (a_{ui} - \hat{a}_{ui})^2 + \lambda \left(\sum_{u=1}^{N_U} \|\mathbf{m}_u\|^2 + \sum_{i=1}^{N_O} \|\mathbf{n}_i\|^2 \right), \quad (19)$$

where w_{ui} is the weight of a_{ui} , and λ denotes the regularization strength to prevent over-fitting.

To optimize the regression model, i.e., (19), we use the Alternating Least Square (ALS) method [51]. With respect to Metaverse user semantic vector \mathbf{m}_u , minimizing J in (19) is equivalent to minimizing [50]

$$J_u = \|\mathbf{W}^u (\mathbf{a}_u - \mathbf{N} \mathbf{m}_u)\|^2 + \lambda \|\mathbf{m}_u\|^2, \quad (20)$$

where \mathbf{W}^u is an $N_O \times N_O$ diagonal matrix, where the $(i_{\text{th}}, i_{\text{th}})$ element in \mathbf{W}^u is w_{ui} . To minimize (20), we let the first-order derivative of J_u be equal to 0, and obtain

$$\frac{\partial J_u}{\partial \mathbf{m}_u} = 2\mathbf{N}^T \mathbf{W}^u \mathbf{N} \mathbf{m}_u - 2\mathbf{N}^T \mathbf{W}^u \mathbf{a}_u + 2\lambda \mathbf{m}_u = 0. \quad (21)$$

Thus, the corresponding \mathbf{m}_u can be solved from (21) as

$$\mathbf{m}_u = (\mathbf{N}^T \mathbf{W}^u \mathbf{N} + \lambda \mathbf{I})^{-1} \mathbf{N}^T \mathbf{W}^u \mathbf{a}_u, \quad (22)$$

where \mathbf{I} is the identity matrix. Next, we can fix \mathbf{m}_u and solve \mathbf{n}_i by following the same process.

However, updating semantic vectors constrains the performance of ALS. To increase the processing speed for supporting online prediction, one solution is to optimize parameters at the element level. By optimizing each coordinate of the semantic vector while leaving the others fixed [52], the computing speed can be greatly increased. Let m_{uf} and n_{if} denote the f_{th} element in \mathbf{m}_u and \mathbf{n}_i , respectively. With respect to m_{uf} , we obtain the derivative of (20) as

$$\frac{\partial J_u}{\partial m_{uf}} = 2 \left(m_{uf} \sum_{i=1}^N w_{ui} n_{if}^2 - \sum_{i=1}^N (a_{ui} - \hat{a}_{ui}^f) w_{ui} n_{if} + \lambda m_{uf} \right), \quad (23)$$

where \hat{a}_{ui}^f denotes the predicted element without the component of latent factor f , which means $\hat{a}_{ui}^f = \hat{a}_{ui} - m_{uf} n_{if}$. Letting $\frac{\partial J_u}{\partial m_{uf}} = 0$, we obtain the solution of m_{uf} as

$$m_{uf} = \frac{\sum_{i=1}^N (a_{ui} - \hat{a}_{ui}^f) w_{ui} n_{if}}{\sum_{i=1}^N w_{ui} n_{if}^2 + \lambda}. \quad (24)$$

Algorithm 1 The user-object-attention values prediction algorithm.

Input: The sparse matrix with empty user-object-attention values, i.e., \mathbf{A} , such as shown in Fig. 7, the semantic factor S , regularization strength λ .

Output: The predicted user-object-attention matrix without empty elements.

```

1: Initialize randomly  $M$  and  $N$ 
2: Obtain the set of user-object pairs whose values are non-zero from  $\mathbf{A}$  as  $\mathcal{A}$ 
3: for Every  $(u, i) \in \mathcal{A}$  do
4:   Calculate (18) to obtain  $\hat{a}_{ui}$ 
5: while Estimation error is larger than the threshold do
6:   ( Update the semantic vector of users )
7:   for  $u = 1, \dots, N_U$  do
8:     for  $f = 1, \dots, S$  do
9:       for  $i \in \mathcal{A}_u$  do
10:         $\hat{a}_{ui}^f \leftarrow \hat{a}_{ui} - m_{uf} n_{if}$ 
11:       Calculate (24) to obtain  $m_{uf}$ 
12:       for  $i \in \mathcal{A}_u$  do
13:         $\hat{a}_{ui}^f \leftarrow \hat{a}_{ui} + m_{uf} n_{if}$ 
14:   ( Update the semantic vector of objects )
15:   for  $i = 1, \dots, N_O$  do
16:     for  $f = 1, \dots, S$  do
17:       for  $u \in \mathcal{A}_i$  do
18:         $\hat{a}_{ui}^f \leftarrow \hat{a}_{ui} - m_{uf} n_{if}$ 
19:       Calculate (25) to obtain  $n_{if}$ 
20:       for  $u \in \mathcal{A}_i$  do
21:         $\hat{a}_{ui}^f \leftarrow \hat{a}_{ui} + m_{uf} n_{if}$ 
22: return  $M \cdot N$ .
```

Then, n_{if} can be derived by following the same method as

$$n_{if} = \frac{\sum_{u=1}^M (a_{ui} - \hat{a}_{ui}^f) w_{ui} m_{uf}}{\sum_{i=1}^M w_{ui} m_{uf}^2 + \lambda}. \quad (25)$$

The detail is shown in **Algorithm 1**.

We analyze the complexity of **Algorithm 1**. If we use the ALS method with the help of (21) and (22), time complexity is high because of the Matrix inversion operation, which can be expressed as $\mathcal{O}(S^3)$ [53]. Considering that updating one semantic vector of Metaverse user has the complexity of $\mathcal{O}(S^3 + N_O S^2)$, we can express the overall time complexity that updates all parameters once as $\mathcal{O}((N_O + N_U) S^3 + N_U N_O S^2)$. Fortunately, by using (24) and (25), we can avoid the matrix inversion operation and reach the complexity of $\mathcal{O}(N_U N_O S^2)$ for one iteration. Furthermore, if the CBS can pre-compute \hat{r}_{ui} , \hat{r}_{ui}^f can be obtained with the complexity of $\mathcal{O}(1)$. Thus, the complexity of **Algorithm 1** is further reduced to $\mathcal{O}(N_U N_O S)$, which can support online user-object-attention predictions. Note that although many more sophisticated machine learning-based methods can be applied to obtain potentially more accurate predictions, our method is simple and fast, and can support achieving QoE close to the upper limit. Specifically, in Section VI, we show that the achieved QoE is only 2% lower than that when all user-object-attention values are perfectly known.

2) *Optimal Rendering Capacity Allocation:* Let $P_k^{(R)}$ denote the total rendering capacity allocated to one virtual

scenario chosen by the k_{th} user. The sum of resolutions set for each virtual object cannot be larger than $P_k^{(R)}$. We then design the optimal rendering capacity allocation scheme by solving the maximization problem as follows:

$$\begin{aligned} & \max_{P_{1,k}^{(R)}, \dots, P_{N_{O,k},k}^{(R)}} \sum_{n=1}^{N_{O,k}} K_{n,k} \ln \left(\frac{P_{n,k}^{(R)}}{P_{\text{th}}^{(R)}} \right) \\ & \text{s.t.} \quad \begin{cases} P_{n,k}^{(R)} > P_{\text{th}}^{(R)}, \forall n, \\ \sum_{n=1}^{N_{O,k}} P_{n,k}^{(R)} \leq P_k^{(R)}. \end{cases} \end{aligned} \quad (26)$$

When one user chooses a Metaverse service, the user-object-attention values $K_{n,k}$ can be predicted with the help of **Algorithm 1**. Then we derive the optimal rendering capacity allocation scheme.

Proposition 1. *To maximize the MI, the rendering capacity for each object in Metaverse xURLLC services is allocated as*

$$P_{n,k}^{(R)*} = \max \left\{ K_{n,k} \frac{1}{\mu^*}, P_{\text{th}}^{(R)} \right\}, \quad (27)$$

where μ^* is obtained by solving the following function

$$\sum_{n=1}^{N_{O,k}} \max \left\{ K_{n,k} \frac{1}{\mu^*}, P_{\text{th}}^{(R)} \right\} = P_k^{(R)}. \quad (28)$$

Proof: Please refer to Appendix D. ■

With the help of Proposition 1, we propose the optimal rendering capacity allocation algorithm as shown in Algorithm 2. Since the number of iterations of **Algorithm 2** is equal to the number of objects that are allocated with the minimal rendering capacity, i.e., $P_{\text{th}}^{(R)}$, Algorithm 2 can converge efficiently and output the optimal rendering capacity allocation scheme.

Algorithms 1 and 2 form the attention-aware rendering capacity allocation algorithm. Thus, the InP can make better use of resources in the wireless MIMO network to provide Metaverse xURLLC services.

V. QOE ANALYSIS AND CONTRACT SOLUTION

In addition to the personalized attention-aware rendering power allocation scheme for xURLLC discussed, we have to derive the expressions for URLLC KPIs, i.e., downlink data rate and uplink BEP, under the considered wireless MIMO network to obtain the closed-form MI expression. Then, we analyze the convexity and discuss the contract solution.

A. URLLC KPIs Analysis

To obtain the analytical expression and investigate the convexity of MI, we derive the closed-form expressions of $R_k^{(D)}$ and $P_k^{(U)}$, respectively.

1) *Downlink Data Rate:* Following the analysis in Section III-A, we can derive the closed-form expression of data rate $R_k^{(D)}$ as follows:

Algorithm 2 The algorithm for allocating the rendering capacity with the help of predicted user-object-attention values.

Input: The predicted user-object-attention values from **Algorithm 1**, $K_{n,k}$, and the total rendering capacity, $P_k^{(R)}$.

Output: The optimal rendering capacity allocation scheme, $P_{1,k}^{(R)}, \dots, P_{N_{Ok},k}^{(R)}$.

- 1: Initialize one temporary variable $j = 1$ and two temporary lists T_1 and T_2
- 2: Start by assuming $P_{n,k}^{(R)*} = K_{n,k} \frac{1}{\mu^*}$ for all n
- 3: Calculate $\mu^* \leftarrow \sum_{n=1}^{N_{Ok}} K_{n,k} / P_k^{(R)}$, and then $P_{n,k}^{(R)*} \leftarrow K_{n,k} / \mu^*$ for every n
- 4: **while** the minimum of $P_{n,k}^{(R)*} < P_{th}^{(R)}$ **do**
- 5: Record $T_1[j] \leftarrow$ the object number of minimal $P_{n,k}^{(R)*}$
- 6: Record $T_2[j] \leftarrow$ the user-object-attention value for the $t_1[j]_{th}$ object
- 7: Re-calculate μ^* and $P_{n,k}^{(R)*}$:
- 8:
$$\mu^* \leftarrow \left(\sum_{n=1}^{N_{Ok}} K_{n,k} - \sum T_2 \right) / \left(P_k^{(R)} - j \times P_{th}^{(R)} \right)$$
- 9: $P_{n,k}^{(R)*} \leftarrow K_{n,k} / \mu^*$ for every n
- 10: **for** temp = 1 : j **do**
- 11: Allocate $P_{th}^{(R)}$ to the $t_1[temp]_{th}$ object:
- 12: $n \leftarrow t_1[temp]_{th}$, $P_{n,k}^{(R)*} \leftarrow P_{th}^{(R)}$
- 13: $j \leftarrow j + 1$
- 14: **return** The optimal rendering capacity allocation scheme $P_{1,k}^{(R)*}, \dots, P_{N_{Ok},k}^{(R)*}$.

Proposition 2. The data rate $R_k^{(D)}$ can be expressed as ²

$$R_k^{(D)} = \frac{B_k \Gamma^{-1}(M_C N_Q)}{\ln(2) \Gamma(M_C M_U)} G_{3,3}^{3,2} \left(\Lambda_k \left| \begin{matrix} 1 - M_C N_Q, 0, 1 \\ M_C M_U, 0, 0 \end{matrix} \right. \right), \quad (29)$$

where B_k is the bandwidth allocated to the k_{th} user, $G_{\cdot, \cdot}^{a, b}(\cdot)$ is the Meijer's G -function [36, eq. (9.301)] and $\Gamma(\cdot)$ is the Gamma function [36, eq. (8.310.1)].

Proof: Please refer to Appendix B. ■

Insights: From the derived data rate, i.e., (29), we can obtain useful insights to guide the URLLC system design. Specifically, when co-channel interference is high in the wireless environment, i.e., $P_{k,q} \rightarrow 0$, we have $\Lambda_k \rightarrow 0$. Equation (29) can be further simplified by calculating the residue at the nearest pole to the Mellin-Barnes integral contour of the Meijer's G -function [36]. Thus, the data rate can be approximated to

$$\hat{R}_k^{(D)} \approx M_C^3 M_U N_Q \frac{B_k \zeta_k D_k^{-\alpha_k} P_k^{(D)} \mu_k}{\ln(2) P_{k,q} \mu_{k,q}}. \quad (30)$$

We can observe that increasing the number of RS antennas can better improve the anti-interference capability of URLLC system compared with increasing the number of CBS antennas.

2) *Uplink Bit Error Probability:* We consider that the frequency division multiplexing is used in the downlink and uplink between CBSs and RSs. For the uplinks, let $P_p^{(U)}$

²To obtain the approximated achievable data rate for xURLLC packets, the short packet transmission can be used to achieve the low latency requirement, which can be addressed in our future work.

denote the co-channel interference, $P_k^{(U)}$ denote the uplink transmit power, $\zeta^{(U)}$ can be calculated by (3), $\mu_k^{(U)}$ and $\mu_p^{(U)}$ denote the channel coefficients for the k_{th} user's links and corresponding interference links, respectively.

The average BEP, $E_k^{(U)}$, under a variety of modulation formats is given by [54]

$$E_k^{(U)} = \int_0^\infty \frac{\Gamma(\tau_2, \tau_1 \gamma)}{2\Gamma(\tau_2)} f_{\gamma_k^{(U)}}(\gamma) d\gamma, \quad (31)$$

where $f_{\gamma_k^{(U)}}$ is the PDF expression of the uplink SIR, i.e., $\gamma_k^{(U)}$, τ_1 and τ_2 are modulation-specific parameters for several modulation and detection scheme combinations, $\Gamma(\tau_2, \tau_1 \gamma) / 2\Gamma(\tau_2)$ represents the conditional bit-error probability, and $\Gamma(\cdot, \cdot)$ denotes the upper incomplete Gamma function [36, eq. (8.350.2)]. When the orthogonal coherent binary frequency-shift keying (BFSK) scheme is used, we set $\{\tau_1 = 0.5, \tau_2 = 0.5\}$. When the antipodal coherent binary phase-shift keying (BPSK) scheme is applied, we have $\{\tau_1 = 1, \tau_2 = 0.5\}$. For the orthogonal non-coherent BFSK scheme, we have $\{\tau_1 = 0.5, \tau_2 = 1\}$. For the antipodal differentially coherent BPSK (DPSK) scheme, we set $\{\tau_1 = 1, \tau_2 = 1\}$.

Proposition 3. The uplink BEP is given by

$$E_k^{(U)} = \frac{\Gamma^{-1}(M_U N_Q)}{2\Gamma(\tau_2) \Gamma(M_C M_U)} G_{4,1}^{1,3} \left(\Lambda_k^{(U)} \left| \begin{matrix} 1 - M_U N_Q, 1, 1 - \tau_2 \\ M_C M_U, 0 \end{matrix} \right. \right), \quad (32)$$

where

$$\Lambda_k^{(U)} = \frac{P_p^{(U)} \mu_p^{(U)}}{M_U \zeta^{(U)} P_k^{(U)} \mu_k^{(U)}}. \quad (33)$$

Proof: Please refer to Appendix C. ■

Insights: Similar to our analysis in Section V-A1, when the co-channel interference is high, we consider that $\Lambda_k^{(U)}$ in (32) approaches 0, which leads to $E_k^{(U)}$ converging to 0.5. Considering that high transmit power is typically used in URLLC to achieve low latency communication [5], we consider the case when $P_k^{(U)} \rightarrow \infty$. According to the properties of the Meijer's G -function [36], we have

$$\hat{E}_k^{(U)} \approx \frac{\Gamma(M_C M_U + \tau_2) \Gamma^{-1}(\tau_2)}{2M_C M_U B(M_U N_Q, M_C M_U)} \left(\frac{\Lambda_k^{(U)}}{\tau_1} \right)^{M_C M_U}. \quad (34)$$

We can observe that the decrease in BEP due to the increase in transmit power is proportional to the product of the numbers of RS and CBS antennas.

B. Convexity Analysis

Considering that \mathcal{M}_k appears in the utility functions of both the MSP and the InP, we study the convexity of \mathcal{M}_k to several resources, i.e., downlink transmit power $P_k^{(D)}$, downlink bandwidth B_k , uplink transmit power $P_k^{(U)}$, and rendering capacity $P_k^{(R)}$, with the help of derived equations in Propositions 2 and 3. Because Λ_k in (2) is a function of $P_k^{(D)}$ and $\Lambda_k^{(U)}$ in (33) is a function of $P_k^{(U)}$, we first derive Lemma 1 that is useful for the analysis of \mathcal{M}_k .

Lemma 1. Let $x \triangleq P_k^{(D)}$, $y \triangleq P_k^{(U)}$ and $\forall \theta \in [0, 1]$ denote a real number. Then, we have $(\Lambda_k(x))^s$ ($-1 < s < 0$) and $(\Lambda_k^{(U)}(y))^t$ ($t > 0$) which satisfy the following inequalities:

$$(\Lambda_k(\theta x_1 + (1 - \theta)x_2))^s \geq \theta \Lambda_k^s(x_1) + (1 - \theta) \Lambda_k^s(x_2), \quad (35)$$

and

$$(\Lambda_k^{(U)}(\theta y_1 + (1 - \theta)y_2))^t \leq \theta \Lambda_k^t(y_1) + (1 - \theta) \Lambda_k^t(y_2), \quad (36)$$

respectively.

Proof: Please refer to Appendix E. ■

Using Lemma 1, we can analyze the convexity of \mathcal{M}_k .

Proposition 4. The MI of the k_{th} user, \mathcal{M}_k , is linear to the downlink bandwidth B_k , and concave in the downlink transmit power $P_k^{(D)}$, the uplink transmit power $P_k^{(U)}$, and the rendering capacity $P_k^{(R)}$.

Proof: Please refer to Appendix F. ■

With the expressions for the downlink data rate and the uplink BEP and the convexity analysis, we can obtain the closed-form MI expression. Thus, the optimal contract can be solved numerically.

C. Contract Solution

We first consider the IC constraint. The closed-form expression of MI can be obtained by substituting (29) and (32) into (17). The InP's utility is concave in Θ , since the MI is concave in the resources as we discussed in Section V-A. For a given contract $\{F_s, u_M\}$, with the help of **Algorithms 1** and **2**, we can use convex optimization tools to obtain the optimal resource allocation scheme and corresponding \mathcal{M}_i . Accordingly, we substitute the IR constraint with the optimal amount of resource and simplify the MSP's maximization problem. The optimal contract, $\{F_s^*, u_M^*\}$, can be also solved using the convex method. We show the MI values obtained under the optimal resource allocation schemes for different contract designs in Fig. 1 (Part IV). Detailed discussion is given in Section VI.

VI. NUMERICAL RESULTS

In this section, we first introduce the UOAL dataset [18], and then present analytical results to illustrate the proposed Metaverse xURLLC service framework. System-wide simulation is left for our future research direction.

A. Metaverse Dataset Preparation

In Metaverse context, we consider a virtual travel scenario, where the user clearly cannot simultaneously see all objects to be displayed, e.g., in VR, and the user's attention is unevenly distributed among the objects that are seen at the same time. This process is similar to that the users view a subset of images. Different users' attention to different objects contained in the images is different because of the users' personal interest. Therefore, we use the UOAL dataset [18], which is composed of 1,000 images, 96 different types of objects, 30 users' attention values to every object. Specifically, some

examples for object labels and the user-object-attention values in UOAL are shown in Fig. 5. If we let all users see all the images in UOAL, we can obtain the ground truth of the user-object-attention records as shown in Fig. 6, which is not given in [18]. To simulate a Metaverse xURLLC service, we generate sparse attention records between users and objects. All the images are divided into small groups, where each group represents one Metaverse virtual scenario option. By letting users select randomly the options and see a random number of images, e.g., due to different virtual travel routes in the Metaverse xURLLC services, we obtain the sparse user-object-attention records as shown in Fig. 7 that is also the input to **Algorithm 1**. The process of using UOAL to obtain the sparse records is given in Appendix A.

B. Performance Analysis

To answer the three questions we presented in Section I, we show the performance of the proposed schemes, including the attention-aware resource allocation scheme, i.e., user-object-attention values prediction in **Algorithm 1** and optimal rendering capacity allocation in **Algorithm 2**, and optimal contract design.

1) *The accuracy of the attention-aware user-object-attention values prediction **Algorithm 1** (for Q3):* : To show the accuracy of **Algorithm 1**, we first randomly generate the user-object-attention sparse matrix as shown in Fig. 7, where 41.8% of the elements are empty, as the input to **Algorithm 1**. Figure 8 shows the user-object-attention prediction error values, i.e., the absolute values of the difference between the predicted results and ground truth (Fig. 6). In Fig. 8, we observe that 67.2% of the prediction error values are 0, 30.7% of the error values are 1, and only 2.12% of the error values are 2. If we consider only the values that are unknown in the input matrix, we can observe that 62.8% of the error values are 0, 34.1% of the error values are 1, and 3.16% of the error values are 2. Thus, we conclude that **Algorithm 1** can help to predict the user-object-attention values accurately. In the following discussion, we show that the predicted values can be used to achieve QoE close to the theoretical upper bound.

2) *The effectiveness of the optimal rendering capacity allocation **Algorithm 2** (for Q3):* : Figure 1 (Part III) illustrates the MI of 30 users under three different allocation schemes, i.e., random, uniform (conventional URLLC without considering the attention differences among users), attention-aware rendering capacity allocation (xURLLC), and the upper-bound obtained from the ground truth. The resolution (K) is used as the measure of rendering capacity³. We consider that the minimal rendering capacity threshold for one virtual object, i.e., $P_{\text{th}}^{(R)}$, is 15 K. The total rendering capacity for the i_{th} user is $N_{O_i} \times 20$ K, where N_{O_i} is the number of virtual objects. We consider that the MSP has the sparse user-object-attention values matrix, i.e., Fig. 7. The Metaverse scenario options are then selected randomly by users according to **Algorithm 3**, and then different resource allocation schemes are

³Here we define that 1 K resolution refers to 960×480 pixel resolution [55]. It is suggested that the resolution should be above 12 K to obtain the ideal-experience [55].

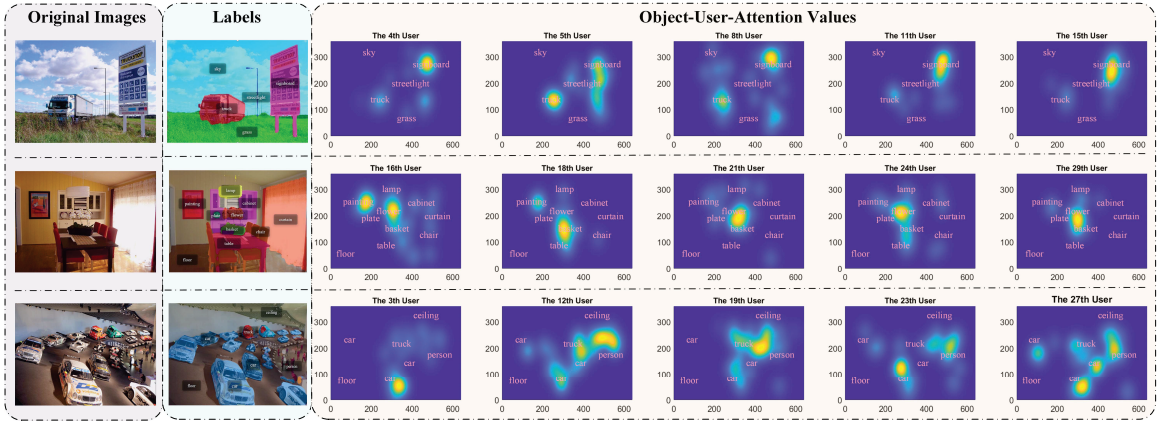


Fig. 5. Some examples for object labels and the user-object-attention values in UOAL [18].

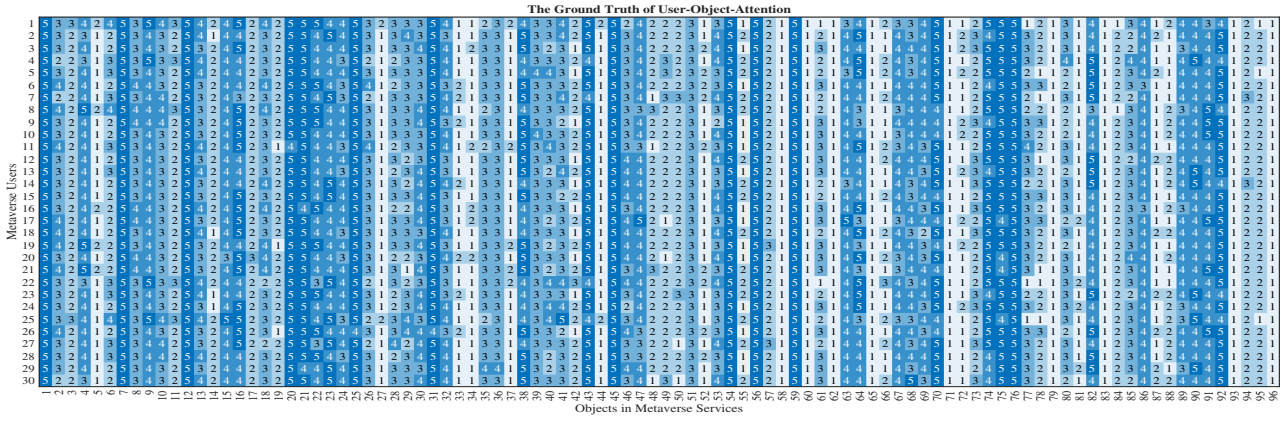


Fig. 6. The ground truth of the user-object-attention records, which is obtained by letting every user see every images in UOAL.

used. Specifically, the random and uniform rendering capacity allocation scheme distribute the rendering capacity randomly and uniformly, respectively, while ensuring that each object is assigned with the minimum threshold $P_{th}^{(R)}$. For the attention-aware scheme, the MSP predicts the user-object-attention values with the help of **Algorithm 1** to obtain $K_{n,k}$. Thus, the rendering capacity is allocated with the help of **Algorithm 2**. The upper-bound is obtained with the help of ground truth user-object-attention values and **Algorithm 2**. From Fig. 1 (Part III), we can observe that the xURLLC attention-aware rendering capacity allocation scheme can achieve a maximum of 25.5%, a minimum of 6.26% and an average of 20.1% MI improvement compared to the URLLC uniform rendering capacity allocation scheme. Moreover, the theoretical upper-bound has only a 2% QoE improvement compared to the attention-aware scheme. This verifies the effectiveness of our proposed optimal rendering capacity allocation **Algorithm 2**.

3) *The superiority of the xURLLC over conventional URLLC (for Q2 and Q3):* Considering that the QoE expression contains the objective KPIs, i.e., downlink data rate and uplink BEP, which are affected by the wireless transmission in the MIMO network, we consider three Metaverse users with the parameters that are given in Table II. The analytical results of downlink data rate and uplink BEP are obtained from (29) and (32), respectively. Perfect agreement is observed between

TABLE II
NETWORK PARAMETERS FOR 3 METAVERSE USERS.

Parameters	1 st User	2 nd User	3 rd User
Number of antennas in CBS, M_C	6		
Number of antennas in RS, M_U	3	7	
Number of co-channel interference, N_Q	3		
Power of interference links, $P_{k,p}$	5 dBW		1 dBW
Channel coefficient of interference links, $\mu_{k,p}$	-3 dB	-1 dB	-3 dB
Channel coefficient of data links, μ_k	-1 dB	-2 dB	-1 dB
Distance between CBS and RS, D_k	10 m	6 m	10 m
Path loss exponent, α_k	2		

analytical results and Monte Carlo simulations, thus validating our derivations. Furthermore, we can observe the impacts of different network parameters on users' wireless connections. Specifically, Table II shows that the 2nd user is in a better quality wireless environment than the 1st user. As show in Fig. 9, compared with the 1st user, the 2nd user has a higher downlink data rate and a lower uplink BEP under the same

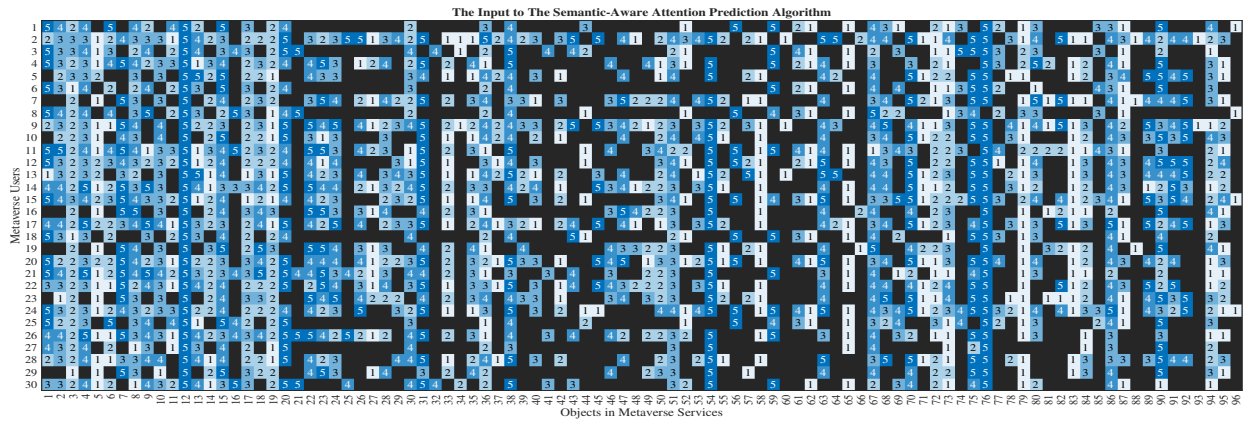


Fig. 7. The sparse user-object-attention records obtained by randomly selecting the virtual scenarios options for each user, and randomly reserving the images as the freely-selected travel path for each user.

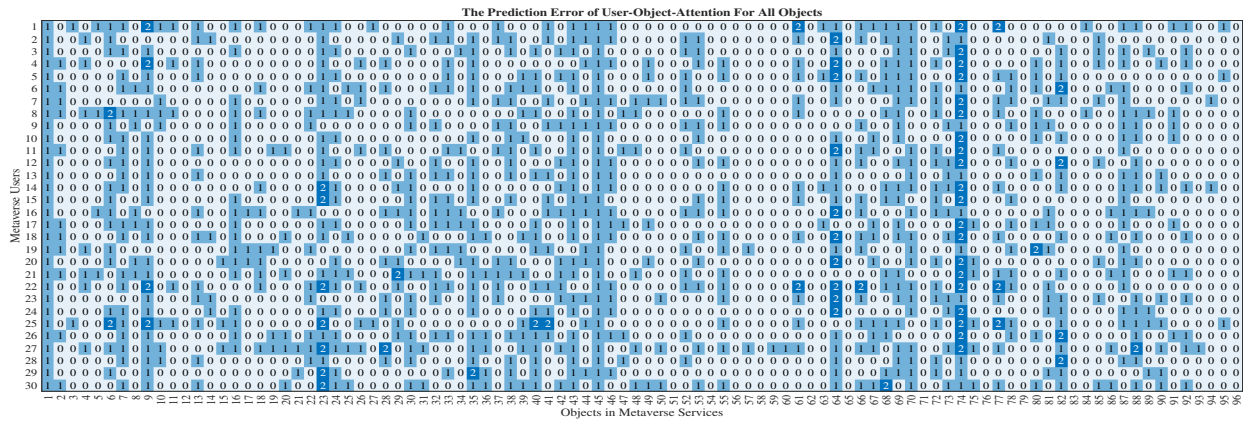


Fig. 8. The prediction error of user-object-attention values for all objects.

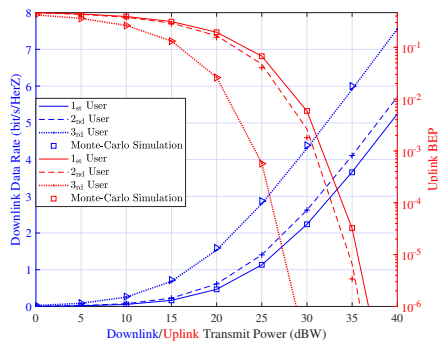


Fig. 9. Conventional URLLC KPIs in the Meta-Immersion expression, i.e., downlink data rate and uplink BEP, for three users versus the downlink and uplink transmit power, respectively.

transmit power. Hardware facilities also affect the wireless connections. The RS serving the 3th user is equipped with the maximum number of antennas, thus allowing the 3th user to achieve the best performance. Fortunately, in the MIMO wireless network, satisfactory URLLC KPIs can always be achieved when the transmit power is high. However, conventional URLLC that does not utilize the uneven user attention in novel Metaverse services to achieve personalized rendering

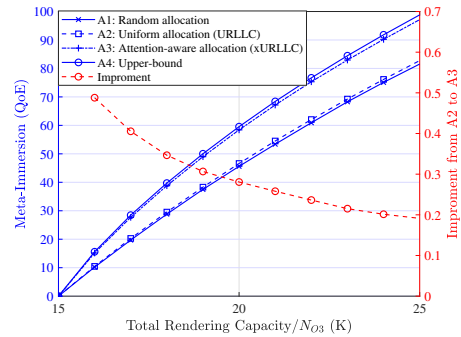


Fig. 10. Meta-Immersion of the 3rd user versus the total rendering capacity, under three different resource allocation schemes, and the upper-bound obtained using the ground truth user-object-attention values.

capability allocation would bring users lower QoE values than xURLLC. To show this, we focus on the 3rd user in Fig. 1 (Part III). For the virtual scenario option selected randomly by the 3rd user, there are $N_{O3} = 56$ objects. Figure 10 plots the MI of the 3rd user versus the total rendering capacity/ N_{O3} under three different resource allocation schemes and the upper-bound obtained from the ground truth. An interesting insight is that the attention-aware scheme brings a higher percentage of improvement compared to the uniform allocation

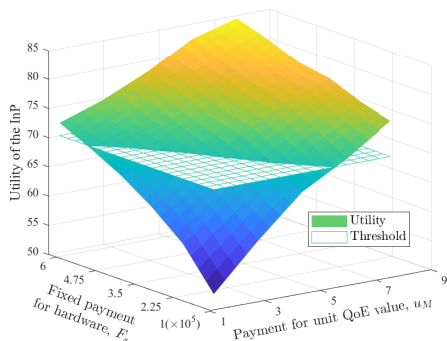


Fig. 11. The utility of the InP versus the payment from the MSP to the InP for unit QoE value, u_M , and the fixed payment from the MSP for using the hardware infrastructures, F_s .

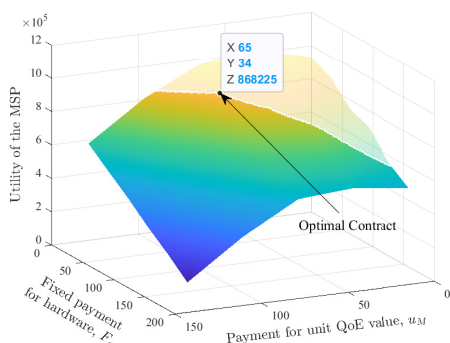


Fig. 12. The utility of the MSP versus the payment from the MSP to the InP for unit QoE value, u_M , and the fixed payment from the MSP for using the hardware infrastructures, F_s .

when the total resources are constrained, i.e., when the total rendering capacity is small. This shows that the attention-aware scheme can improve resource utilization efficiency and thus bring a better Metaverse experience to users.

4) *The effectiveness of the optimal contract design (for QI)*: We then study the optimal contract design problem in the Metaverse xURLLC service market. Figs 1 (Part IV), 11 12 depict the MI, utilities of the InP and the MSP versus the payment from the MSP to the InP for unit QoE value u_M and the fixed payment from the MSP for using the hardware infrastructures F_s , respectively, with the network parameters for 3 Metaverse users as shown in Table II, $U_{th}^{InP} = 70$, $\tau = 0.8$, $R_{k,max}^{(D)} = 42$ Mbit/s, $R_{k,min}^{(D)} = 10$ Mbit/s, $E_{k,min}^{(U)} = 10^{-2}$, $E_{k,min}^{(D)} = 10^{-8}$, and the unit prices for rendering capacity (per K), downlink transmit power (per kW), downlink bandwidth (per MHz), uplink power (per kW), are denoted by $\Theta = \{5, 3, 2, 4\}$. Specifically, Fig. 11 shows the IC constraint. For a given contract $\{F_s, u_M\}$, the InP optimizes its utility function based on the price of various resources and the contract. An interesting insight is that the optimal resource allocation scheme that leads to the maximal MI is only related to u_M rather than F_s . The reason is that F_s is an additive term in the utility of the InP, (12), which is independent of MI. However, it is clear that F_s impacts the value of the InP's utility function and the IR constraint. From Fig. 11, we

can observe that the increase of both u_M and F_s leads to an increase in utility. Because of the IR constraint, the utility of the InP must be larger than a threshold, U_{th}^{InP} , which makes the contracts with small values of F_s and u_M not available. Thus, the value of F_s cannot be zero. The optimal contract obtained by maximizing the utility of the MSP under IC and IR constraints is shown in Fig. 12. We can observe that the utility of the MSP under the optimal contract decreases as the U_{th}^{InP} required by the InP increases. However, the optimal contract scheme, i.e., the marked point in Fig. 12, can always achieve the highest utility values for both the InP and the MSP, compared with other feasible contract schemes. This verifies the effectiveness of the optimal contract design.

VII. CONCLUSION AND FUTURE DIRECTIONS

To deploy Metaverse xURLLC services in the wireless MIMO network, we proposed a contract design framework between the MSP and the InP. The utility of the MSP was maximized while ensuring the QoE of users, i.e., KPI of the xURLLC service, and the incentives of the InP. To consider both the objective KPIs and the subjective feelings of Metaverse users, we proposed a novel metric, i.e., MI, to define formally the QoE for next-generation Internet services such as Metaverse xURLLC. By analyzing the objective network performance indicators and subject user attention values, the closed-form expression of MI was derived. Considering that the historical user-object-attention records in the Metaverse service are sparse, we designed the attention-aware rendering capacity allocation algorithm that can predict the attention values first and then allocate resources optimally. Using the UOAL dataset, we verified that the MI can be increased averagely by 20.1% by the xURLLC attention-aware allocation scheme compared to the conventional URLLC uniform allocation scheme.

We list potential future research directions as follows:

- *Cold-start in Metaverse services*: In this paper, we use sparse user-object interaction records to predict user attention. However, the cold-start problem exists when the users are new. To enable personalized resource allocation scheme for any user without collecting extra user information beforehand, cold-start problem has to be addressed. A possible solution is to use graph neural networks to perform interest prediction from the user's current Metaverse services [18].
- *Attention-aware cross-layer design*: We focus on using the user attention mechanism to guide the upper-layer resource allocation scheme design. As emerging physical layer access technologies, e.g., extremely large-scale MIMO [54], are increasingly being applied, cross-layer design schemes can be investigated to achieve URLLC and further improve the QoE. For example, the accuracy of the beamforming scheme can be dynamically adjusted according to the Metaverse service content.
- *Secure Metaverse services*: We derive the downlink data rate and the uplink BEP for the MIMO technique to provide Metaverse services. However, data in the wireless environment can be easily eavesdropped, thus posing

a privacy risk to users. To achieve secure wireless network-enabled Metaverse services, physical layer security, covert communication, and encryption techniques can be applied [56].

APPENDIX A DATASET PREPARATION

The algorithm that is used to obtain the sparse records are given in Algorithm 3 in Python style.

Algorithm 3 Generating sparse user-object-attention records for the k_{th} user in Metaverse xURLLC service.

```
# G, E, L: grouped images, eye-movement records
# and segmentation labels, all in array format
# a1: random int range [2, 4]
# a2: random float range [0.3, 0.7]

# randomly select a1 groups
G_k, E_k, L_k = selet_data(G, E, L, a1)
# randomly reserve a2 of data
G_k, E_k, L_k = reserve_data(G_k, E_k, L_k, a2)

scores = []
for j in object_list:
# count the frequency of object j
c_j = count_frequency(j, G_k)

# find the positions of j on segmentations
pos_j = numpy.where(L_k==j)

# compute attention score of j
s_j = E_k[pos_j].sum()/c_j

scores.append(s_j)

# split scores into 5 levels
levels = numpy.array_split(scores.sort(), 5)
# map raw values to 5 levels
scores_k = map_level(scores, levels)
```

APPENDIX B PROOF OF PROPOSITION 2

The downlink data rate per Hertz is defined as

$$R_k^{(B)} \triangleq R_k^{(D)} / B_k = \int_0^\infty \log_2(1 + \gamma) f_{\gamma_k}(\gamma) d\gamma. \quad (\text{B-1})$$

Substituting (1) into (B-1), we can obtain

$$R_k^{(B)} = \frac{\Lambda_k^{M_C M_U}}{B(M_C M_U, M_C N_Q)} \times \int_0^\infty \frac{\log_2(1+x) x^{M_C M_U - 1}}{(1+x\Lambda_k)^{M_C M_U + M_C N_Q}} dx. \quad (\text{B-2})$$

With the help of [57, eq. (01.04.07.0003.01)], the logarithmic function in (B-2) can be re-written as

$$\log_2(1+x) = \frac{1}{2\pi i} \int_{\mathcal{L}_1} \frac{\Gamma(s+1)\Gamma^2(-s)x^{-s}}{\Gamma(1-s)\ln 2} ds, \quad (\text{B-3})$$

where the integration path of \mathcal{L}_1 goes from $s-i\infty$ to $s+i\infty$, s is a real number, $-1 < s < 0$ and $i = \sqrt{-1}$. Then, the $R_k^{(B)}$ can be expressed as

$$R_k^{(B)} = \frac{\Lambda_k^{M_C M_U}}{B(M_C M_U, M_C N_Q)} \frac{1}{2\pi i} \int_{\mathcal{L}_1} \frac{\Gamma(s+1)\Gamma^2(-s)}{\Gamma(1-s)} I_C ds, \quad (\text{B-4})$$

where

$$I_C = \int_0^\infty \frac{x^{M_C M_U - 1 - s}}{(1+x\Lambda_k)^{M_C M_U + M_C N_Q}} dx. \quad (\text{B-5})$$

According to [36, eq. (3.194.3)], the I_C can be solved as [58]

$$I_C = \Lambda_k^{s-M_C M_U} \frac{\Gamma(M_C M_U - s)\Gamma(s + M_C N_Q)}{\Gamma(M_C M_U + M_C N_Q)}. \quad (\text{B-6})$$

By combining (B-6) and (B-4), we can obtain

$$R_k^{(B)} = \frac{1}{\Gamma(M_C M_U)\Gamma(M_C N_Q)} \frac{1}{2\pi i} \times \int_{\mathcal{L}_1} \frac{\Gamma^2(-s)\Gamma(s + M_C N_Q)\Gamma(s+1)}{\Gamma^{-1}(M_C M_U - s)\Gamma(1-s)} \Lambda_k^s ds. \quad (\text{B-7})$$

With the help of [36, eq. (9.301)] and (B-1), we derive the closed-form $R_k^{(D)}$ as (29), which completes the proof.

APPENDIX C PROOF OF PROPOSITION 3

Using the definition of Gamma function [36, eq. (8.350)], we can re-write $E_k^{(U)}$ as

$$E_k^{(U)} = \frac{\tau_1 \tau_2}{2\Gamma(\tau_2)} \int_0^\infty x^{\tau_2 - 1} e^{-\tau_1 x} F_{\gamma_k^{(U)}}(x) d\gamma, \quad (\text{C-1})$$

where $F_{\gamma_k^{(U)}}$ is the CDF expression for the uplink SIR, $\gamma_k^{(U)}$. We first derive $F_{\gamma_k^{(U)}}$. Using the definition of CDF, we have

$$F_{\gamma_k^{(U)}}(\gamma) = \int_0^\gamma f_{\gamma_k^{(U)}}(x) dx. \quad (\text{C-2})$$

Replacing $M_C N_Q$ with $M_U N_Q$ and substituting (1) into (C-2), we then solve the integration part with the help of [36, eq. (3.194)] and obtain

$$F_{\gamma_k^{(U)}}(\gamma) = \frac{\Lambda_k^{(U)M_C M_U}}{B(M_C M_U, M_U N_Q)} \frac{\gamma^{M_C M_U}}{M_C M_U} \times {}_2F_1\left(M_C M_U + M_U N_Q, M_C M_U; 1 + M_C M_U; \frac{\Lambda_k^{(U)}}{-\gamma}\right), \quad (\text{C-3})$$

where ${}_2F_1(\cdot, \cdot; \cdot; \cdot)$ is the Gauss hypergeometric function [36, eq. (9.111)]. With the help of [36, 9.113] and [36, 8.331.1], the CDF can be expressed as

$$F_{\gamma_k^{(U)}}(\gamma) = \frac{1}{\Gamma(M_C M_U)\Gamma(M_U N_Q)} \frac{1}{2\pi i} \times \int_{\mathcal{L}_2} \frac{\Gamma(M_U N_Q + t)\Gamma(t)}{\Gamma^{-1}(M_C M_U - t)\Gamma(1+t)} \left(\Lambda_k^{(U)}\gamma\right)^t dt, \quad (\text{C-4})$$

where the integration path of \mathcal{L}_2 goes from $t-i\infty$ to $t+i\infty$, t is a real number, and $t > 0$. Substituting (C-4) into (C-1),

the BEP can be written as

$$E_k^{(U)} = \frac{\tau_1^{\tau_2} \Gamma^{-1}(M_U N_Q)}{2\Gamma(\tau_2) \Gamma(M_C M_U)} \frac{1}{2\pi i} \times \int_{\mathcal{L}_2} \frac{\Gamma(M_U N_Q + t) \Gamma(t)}{\Gamma^{-1}(M_C M_U - t) \Gamma(1 + t)} \Lambda_k^{(U)t} I_D dt, \quad (\text{C-5})$$

where

$$I_D = \int_0^\infty x^{t+\tau_2-1} e^{-\tau_1 x} dx. \quad (\text{C-6})$$

With the help of [36, eq. (3.351.3)] and [36, eq. (8.339.1)], I_D can be solved as

$$I_D = \Gamma(t + \tau_2) \tau_1^{-t-\tau_2}. \quad (\text{C-7})$$

Substituting I_D into (C-5) and using [36, eq. (9.301)], we can derive 32 to complete the proof.

APPENDIX D PROOF OF PROPOSITION 1

The objective function in (26) is convex in the rendering capacity and the strong duality holds for the convex problem according to the Slater's condition [59]. The Lagrangian associated with problem (26) is given by

$$\begin{aligned} F_{\mathcal{L}} &\triangleq F_{\mathcal{L}} \left(P_{1,k}^{(R)}, \dots, P_{N_{Ok},k}^{(R)}, \lambda_1, \dots, \lambda_{N_{Ok}}, \mu \right) \\ &= - \sum_{n=1}^{N_{Ok}} K_{n,k} \ln \left(\frac{P_{n,k}^{(R)}}{P_{\text{th}}^{(R)}} \right) - \sum_{n=1}^{N_{Ok}} \lambda_n \left(P_{n,k}^{(R)} - P_{\text{th}}^{(R)} \right) \\ &\quad - \mu \left(P_k^{(R)} - \sum_{n=1}^{N_{Ok}} P_{n,k}^{(R)} \right), \end{aligned} \quad (\text{D-1})$$

where λ_n ($n = 1, \dots, N_{Ok}$) and μ are the Lagrange multipliers. The Karush–Kuhn–Tucker (KKT) optimality conditions for the optimal solution is

$$\begin{cases} -K_{n,k} + P_{n,k}^{(R)} (\mu - \lambda_n) = 0, \\ P_{n,k}^{(R)} - P_{\text{th}}^{(R)} \geq 0, \\ \lambda_n \geq 0, \\ \lambda_n \left(P_{n,k}^{(R)} - P_{\text{th}}^{(R)} \right) = 0, \\ P_k^{(R)} - \sum_{n=1}^{N_{Ok}} P_{n,k}^{(R)} = 0, \end{cases} \quad (\text{D-2})$$

which leads to

$$\lambda_n = -K_{n,k} \frac{1}{P_{n,k}^{(R)}} + \mu. \quad (\text{D-3})$$

By (D-2) and (D-3), we have two cases for solving optimal $P_{n,k}^{(R)}$ as follows:

Case 1: $\lambda_n > 0$ & $P_{n,k}^{(R)} = P_{\text{th}}^{(R)}$

By solving (D-3), we have $\mu < \frac{-K_{n,k}}{P_{\text{th}}^{(R)}}$.

Case 2: $\lambda_n = 0$ & $P_{n,k}^{(R)} \geq P_{\text{th}}^{(R)}$

By solving (D-3), we have $P_{n,k}^{(R)} = K_{n,k} \frac{1}{\mu} \geq P_{\text{th}}^{(R)}$.

Therefore, it can be inferred from the above two cases that

$$P_{n,k}^{(R)*} = \max \left\{ K_{n,k} \frac{1}{\mu^*}, P_{\text{th}}^{(R)} \right\}, \quad (\text{D-4})$$

where μ^* can be obtained by solving

$$\sum_{n=1}^{N_{Ok}} P_{n,k}^{(R)*} = \sum_{n=1}^{N_{Ok}} \max \left\{ K_{n,k} \frac{1}{\mu^*}, P_{\text{th}}^{(R)} \right\} = P_k^{(R)}. \quad (\text{D-5})$$

Thus, we complete the proof.

APPENDIX E PROOF OF LEMMA 1

We study the convexity of $(\Lambda_k(x))^s$ ($-1 < s < 0$) and $(\Lambda_k^{(U)}(y))^t$ ($t > 0$). By performing the quadratic derivative to x and y , we obtain

$$\frac{\partial^2 (\Lambda_k(x))^s}{\partial x^2} = \left(\frac{P_p \mu_p}{M_U \zeta \mu_k} \right)^s \frac{s(s+1)}{x^{s+2}} < 0, \quad (\text{E-1})$$

and

$$\frac{\partial^2 (\Lambda_k^{(U)}(y))^t}{\partial y^2} = \left(\frac{P_p \mu_p}{M_U \zeta \mu_k} \right)^t \frac{t(t+1)}{x^{t+2}} > 0, \quad (\text{E-2})$$

respectively.

Thus, $(\Lambda_k(x))^s$ is concave and $(\Lambda_k^{(U)}(y))^t$ is convex. With the help of the Jensen's inequality [60], we can derive (35) and (36) to complete the proof.

APPENDIX F PROOF OF PROPOSITION 4

We first focus on $P_k^{(D)}$. Let $x \triangleq P_k^{(D)}$ and $\forall \theta \in [0, 1]$ denote a real number. Using (B-7) in Proposition 2, we have

$$\begin{aligned} R_k^{(B)}(\theta x_1 + (1-\theta)x_2) &= \frac{1}{\Gamma(M_C M_U) \Gamma(M_C N_Q)} \frac{1}{2\pi i} \\ &\times \int_{L_1} \frac{\Gamma^2(-s) \Gamma(s + M_C N_Q) \Gamma(s+1)}{\Gamma^{-1}(M_C M_U - s) \Gamma(1-s)} \\ &\times \Lambda_k^s(\theta x_1 + (1-\theta)x_2) ds. \end{aligned} \quad (\text{F-1})$$

With the help of (35) in Lemma 1, after some mathematical transformations, we obtain

$$R_k^{(B)}(\theta x_1 + (1-\theta)x_2) \geq \theta R_k^{(B)}(x_1) + (1-\theta) R_k^{(B)}(x_2). \quad (\text{F-2})$$

According to the definition of convex function [59], we conclude that $R_k^{(B)}$ is concave in $P_k^{(D)}$. Considering the $\mathcal{T}(\cdot)$ (16) function in \mathcal{M}_k is the linear-fractional function that preserves convexity [59], we can derive that \mathcal{M}_k is concave in $P_k^{(D)}$.

For downlink bandwidth B_k , it is simple to obtain that

$$\frac{\partial^2 \mathcal{M}_k}{\partial B_k^2} = 0, \quad (\text{F-3})$$

which means that \mathcal{M}_k is linear to B_k .

For uplink transmit power $P_k^{(U)}$, let $y \triangleq P_k^{(U)}$. Using Proposition 3 and substituting (C-7) into (C-5), we have

$$\begin{aligned} E_k^{(U)}(\theta y_1 + (1-\theta)y_2) &= \frac{\Gamma^{-1}(M_U N_Q)}{2\Gamma(\tau_2) \Gamma(M_C M_U)} \frac{1}{2\pi i} \\ &\times \int_{\mathcal{L}} \frac{\Gamma(M_U N_Q + t) \Gamma(t) \Gamma(t + \tau_2)}{\Gamma^{-1}(M_C M_U - t) \Gamma(1 + t)} \\ &\times \left(\frac{\Lambda_k^{(U)}(\theta y_1 + (1-\theta)y_2)}{\tau_1} \right)^t dt. \end{aligned} \quad (\text{F-4})$$

Using (36) in Lemma 1, we have

$$E_k^{(U)}(\theta y_1 + (1-\theta)y_2) \leq \theta E_k^{(U)}(y_1) + (1-\theta)E_k^{(U)}(y_2). \quad (\text{F-5})$$

Thus, $E_k^{(U)}$ is convex to $P_k^{(U)}$. Because \mathcal{M}_k is linear to $1 - E_k^{(U)}$, we derive that \mathcal{M}_k is concave in $P_k^{(U)}$ to complete the proof.

REFERENCES

- [1] J. Joshua, "Information bodies: Computational anxiety in neal stephenson's snow crash," *Interdiscip. Lit. Stud.*, vol. 19, no. 1, pp. 17–47, Jan. 2017.
- [2] H. Du, J. Zhang, K. Guan, D. Niyato, H. Jiao, Z. Wang, and T. Kürner, "Performance and optimization of reconfigurable intelligent surface aided THz communications," *IEEE Trans. Commun.*, vol. 70, no. 5, pp. 3575–3593, May 2022.
- [3] S. Verma, Y. Kawamoto, and N. Kato, "A smart Internet-wide port scan approach for improving IoT security under dynamic WLAN environments," *IEEE Internet Things J.*, vol. 9, no. 14, pp. 11 951–11 961, 2021.
- [4] —, "A network-aware Internet-wide scan for security maximization of IPV6-enabled WLAN IoT devices," *IEEE Internet Things J.*, vol. 8, no. 10, pp. 8411–8422, 2020.
- [5] C. She, C. Sun, Z. Gu, Y. Li, C. Yang, H. V. Poor, and B. Vucetic, "A tutorial on ultrareliable and low-latency communications in 6G: Integrating domain knowledge into deep learning," *Proc. IEEE*, vol. 109, no. 3, pp. 204–246, Mar. 2021.
- [6] W. Saad, M. Bennis, and M. Chen, "A vision of 6G wireless systems: Applications, trends, technologies, and open research problems," *IEEE Netw.*, vol. 34, no. 3, pp. 134–142, Mar. 2019.
- [7] C. She, R. Dong, Z. Gu, Z. Hou, Y. Li, W. Hardjawana, C. Yang, L. Song, and B. Vucetic, "Deep learning for ultra-reliable and low-latency communications in 6G networks," *IEEE Netw.*, vol. 34, no. 5, pp. 219–225, May 2020.
- [8] V. Kelkkanen, M. Fiedler, and D. Lindero, "Bitrate requirements of non-panoramic VR remote rendering," in *Proc. ACM Int. Conf. Multimedia*, Oct. 2020, pp. 3624–3631.
- [9] Y. Lu, H. Zheng, S. Chand, W. Xia, Z. Liu, X. Xu, L. Wang, Z. Qin, and J. Bao, "Outlook on human-centric manufacturing towards industry 5.0," *J. Manuf. Syst.*, vol. 62, pp. 612–627, Jan. 2022.
- [10] R. Dong, C. She, W. Hardjawana, Y. Li, and B. Vucetic, "Deep learning for radio resource allocation with diverse quality-of-service requirements in 5G," *IEEE Trans. Wireless Commun.*, vol. 20, no. 4, pp. 2309–2324, Apr. 2020.
- [11] Y. Han, D. Niyato, C. Leung, C. Miao, and D. I. Kim, "A dynamic resource allocation framework for synchronizing metaverse with IoT service and data," *arXiv preprint arXiv:2111.00431*, 2021.
- [12] C. She, P. Cheng, A. Li, and Y. Li, "Grand challenges in signal processing for communications," *Front. Signal Process.*, vol. 1, p. 664331, 2021.
- [13] H. Du, B. Ma, D. Niyato, and J. Kang, "Rethinking quality of experience for metaverse services: A consumer-based economics perspective," *arXiv preprint arXiv:2208.01076*, 2022.
- [14] W. Yang, H. Du, Z. Liew, W. Y. B. Lim, Z. Xiong, D. Niyato, X. Chi, X. S. Shen, and C. Miao, "Semantic communications for 6G future internet: Fundamentals, applications, and challenges," *arXiv preprint arXiv:2207.00427*, 2022.
- [15] H. Du, J. Wang, D. Niyato, J. Kang, Z. Xiong, J. Zhang *et al.*, "Semantic communications for wireless sensing: RIS-aided encoding and self-supervised decoding," *arXiv preprint arXiv:2211.12727*, 2022.
- [16] Y. Zhang and Z. Han, *Contract Theory for Wireless Networks*. Springer, 2017.
- [17] Y. Zhang, Y. Gu, M. Pan, N. H. Tran, Z. Dawy, and Z. Han, "Multi-dimensional incentive mechanism in mobile crowdsourcing with moral hazard," *IEEE Trans. Mobile Comput.*, vol. 17, no. 3, pp. 604–616, Mar. 2017.
- [18] H. Du, J. Wang, D. Niyato, J. Kang, Z. Xiong, X. S. Shen, and D. I. Kim, "Exploring attention-aware network resource allocation for customized metaverse services," *IEEE Netw.*, to appear, 2022.
- [19] A. C. Schütz, D. I. Braun, and K. R. Gegenfurtner, "Eye movements and perception: A selective review," *J. Vision*, vol. 11, no. 5, pp. 9–9, May 2011.
- [20] S. Onat, A. Açık, F. Schumann, and P. König, "The contributions of image content and behavioral relevancy to overt attention," *PLoS One*, vol. 9, no. 4, p. e93254, Apr. 2014.
- [21] E. Bozkir, D. Geisler, and E. Kasneci, "Assessment of driver attention during a safety critical situation in VR to generate VR-based training," in *ACM Symp. Appl. Percept.*, Sept. 2019, pp. 1–5.
- [22] S. Berkovsky, R. Taib, I. Koprinska, E. Wang, Y. Zeng, J. Li, and S. Kleitman, "Detecting personality traits using eye-tracking data," in *Proc. CHI Conf. Hum. Factors Comput. Syst.*, Mar. 2019, pp. 1–12.
- [23] C. Braunagel, D. Geisler, W. Rosenstiel, and E. Kasneci, "Online recognition of driver-activity based on visual scanpath classification," *IEEE Trans. Intell. Transp. Syst.*, vol. 9, no. 4, pp. 23–36, Apr. 2017.
- [24] Y. Feng, G. Cheung, W.-t. Tan, P. Le Callet, and Y. Ji, "Low-cost eye gaze prediction system for interactive networked video streaming," *IEEE Trans. Multimedia*, vol. 15, no. 8, pp. 1865–1879, Aug. 2013.
- [25] G. Ghinea and G.-M. Muntean, "An eye-tracking-based adaptive multimedia streaming scheme," in *Proc. IEEE Int. Conf. Multimedia Expo.*, 2009, pp. 962–965.
- [26] Y. Su, Y. Xu, S. Cheng, C. Ko, and K.-Y. Young, "Development of an effective 3D VR-based manipulation system for industrial robot manipulators," in *Proc. Asian Control Conf. (ASCC)*. IEEE, 2019, pp. 1–6.
- [27] R. Likamwa, J. Hu, V. Kodukula, and Y. Liu, "Adaptive resolution-based tradeoffs for energy-efficient visual computing systems," *IEEE Pervasive Comput.*, to appear, 2021.
- [28] Y. Zhang, M. Pan, L. Song, Z. Dawy, and Z. Han, "A survey of contract theory-based incentive mechanism design in wireless networks," *IEEE Wireless Commun.*, vol. 24, no. 3, pp. 80–85, Mar. 2017.
- [29] L. Gao, X. Wang, Y. Xu, and Q. Zhang, "Spectrum trading in cognitive radio networks: A contract-theoretic modeling approach," *IEEE J. Sel. Areas Commun.*, vol. 29, no. 4, pp. 843–855, Apr. 2011.
- [30] Y. Zhang, L. Song, W. Saad, Z. Dawy, and Z. Han, "Contract-based incentive mechanisms for device-to-device communications in cellular networks," *IEEE J. Sel. Areas Commun.*, vol. 33, no. 10, pp. 2144–2155, Oct. 2015.
- [31] L. Lv, C. Zheng, L. Zhang, C. Shan, Z. Tian, X. Du, and M. Guizani, "Contract and lyapunov optimization-based load scheduling and energy management for UAV charging stations," *IEEE Trans. Green Commun. Netw.*, vol. 5, no. 3, pp. 1381–1394, Mar. 2021.
- [32] K. Wang, W. Chen, J. Li, Y. Yang, and L. Hanzo, "Joint task offloading and caching for massive MIMO-aided multi-tier computing networks," *IEEE Trans. Commun.*, to appear, 2022.
- [33] T. Um, H. Kim, H. Kim, J. Lee, C. Koo, and N. Chung, "Travel incheon as a metaverse: Smart tourism cities development case in Korea," in *ENTER22 E-Tourism Conf*. Springer, Cham, 2022, pp. 226–231.
- [34] C. Tsao and P.-C. Su, "A technical report for visual attention estimation in HMD challenge," in *Prof. Int. Conf. AIVR*, 2021, pp. 143–144.
- [35] L. Zhang, Y. Li, and L. J. Cimini, "Statistical performance analysis for MIMO beamforming and STBC when co-channel interferers use arbitrary MIMO modes," *IEEE Trans. Commun.*, vol. 60, no. 10, pp. 2926–2937, Oct. 2012.
- [36] I. S. Gradshteyn and I. M. Ryzhik, *Table of Integrals, Series, and Products*, 7th ed. Academic Press, 2007.
- [37] R. A. Horn, "The hadamard product," in *Proc. Symp. Appl. Math.*, vol. 40, 1990, pp. 87–169.
- [38] P. Yang, T. Q. Quek, J. Chen, C. You, and X. Cao, "Feeling of presence maximization: mmWave-enabled virtual reality meets deep reinforcement learning," *arXiv preprint arXiv:2107.01001*, 2021.
- [39] A. Nazir, S. Raza, and C.-N. Chuah, "Unveiling facebook: A measurement study of social network based applications," in *Proc. ACM SIGCOMM Int. Meas.*, 2008, pp. 43–56.
- [40] J. Tremewan, "Behavioral economics: Toward a new economics by integration with traditional economics," *Econ. Rec.*, vol. 96, no. 313, pp. 221–221, 2020.
- [41] H. Du, D. Niyato, J. Kang, D. I. Kim, and C. Miao, "Optimal targeted advertising strategy for secure wireless edge metaverse," *arXiv preprint arXiv:2111.00511*, 2021.
- [42] J.-S. Pang and M. Fukushima, "Quasi-variational inequalities, generalized nash equilibria, and multi-leader-follower games," *Comput. Manag. Sci.*, vol. 2, no. 1, pp. 21–56, Jan. 2005.
- [43] S. Dehaene, "The neural basis of the Weber-Fechner law: A logarithmic mental number line," *Trends Cogn. Sci.*, vol. 7, no. 4, pp. 145–147, Apr. 2003.
- [44] S. Bouchard, J. St-Jacques, G. Robillard, and P. Renaud, "Anxiety increases the feeling of presence in virtual reality," *Presence: Teleop. Virt. Environ.*, vol. 17, no. 4, pp. 376–391, Apr. 2008.
- [45] P. Reichl, B. Tuffin, and R. Schatz, "Logarithmic laws in service quality perception: Where microeconomics meets psychophysics and quality of experience," *Telecommun. Syst.*, vol. 52, no. 2, pp. 587–600, Feb 2013.

- [46] P. Reichl, S. Egger, R. Schatz, and A. D'Alconzo, "The logarithmic nature of QoE and the role of the Weber-Fechner law in QoE assessment," in *Proc. IEEE Int. Conf. Commun.*, May 2010, pp. 1–5.
- [47] I. Lubashevsky, "Psychophysical laws as reflection of mental space properties," *Phys. Life Rev.*, vol. 31, pp. 276–303, 2019.
- [48] T. Nishio, R. Shinkuma, T. Takahashi, and N. B. Mandayam, "Service-oriented heterogeneous resource sharing for optimizing service latency in mobile cloud," in *Proc. Int. Mobile Cloud Comput. & Netw. Workshop*, 2013, pp. 19–26.
- [49] Y. Koren, R. Bell, and C. Volinsky, "Matrix factorization techniques for recommender systems," *Computer*, vol. 42, no. 8, pp. 30–37, Aug. 2009.
- [50] Y. Hu, Y. Koren, and C. Volinsky, "Collaborative filtering for implicit feedback datasets," in *Proc. IEEE Intl. Conf. Data Min.*, Dec. 2008, pp. 263–272.
- [51] D. Zachariah, M. Sundin, M. Jansson, and S. Chatterjee, "Alternating least-squares for low-rank matrix reconstruction," *IEEE Signal Process. Lett.*, vol. 19, no. 4, pp. 231–234, Apr. 2012.
- [52] S. Rendle, Z. Gantner, C. Freudenthaler, and L. Schmidt-Thieme, "Fast context-aware recommendations with factorization machines," in *Proc. Intl. ACM SIGIR Conf. Res. Dev. Inf. Retr.*, 2011, pp. 635–644.
- [53] X. He, H. Zhang, M.-Y. Kan, and T.-S. Chua, "Fast matrix factorization for online recommendation with implicit feedback," in *Proc. Intl. ACM SIGIR Conf. Res. Dev. Inf. Retr.*, 2016, pp. 549–558.
- [54] D. Tse and P. Viswanath, *Fundamentals of wireless communication*. Cambridge, U.K., Cambridge Univ. Press, 2005.
- [55] Huawei iLab, "Cloud VR network solution white paper," <https://www.huawei.com/en/news/2018/9/cloud-vr-solution-white-paper>.
- [56] A. Chorti, A. N. Barreto, S. Köpsell, M. Zoli, M. Chafii, P. Sehier, G. Fettweis, and H. V. Poor, "Context-aware security for 6G wireless: The role of physical layer security," *IEEE Commun. Standards Mag.*, vol. 6, no. 1, pp. 102–108, Jan. 2022.
- [57] Wolfram, "The wolfram functions site," <http://functions.wolfram.com>.
- [58] H. Du, J. Zhang, J. Cheng, and B. Ai, "Millimeter wave communications with reconfigurable intelligent surfaces: Performance analysis and optimization," *IEEE Trans. Commun.*, vol. 69, no. 4, pp. 2752–2768, Apr. 2021.
- [59] S. Boyd, S. P. Boyd, and L. Vandenberghe, *Convex optimization*. Cambridge university press, 2004.
- [60] S. S. Dragomir and N. M. Ionescu, "Some converse of Jensen's inequality and applications," *Revue d'Analyse Numérique et de Théorie de l'Approximation*, vol. 23, no. 1, pp. 71–78, Jan. 1994.